1714

Bath, etal., 1983

USGS-OFR-83-377

USGS-OFR-83-377

United States
Department of the Interior
Geological Survey

GEOLOGIC AND GEOPHYSICAL INVESTIGATIONS OF CLIMAX STOCK INTRUSIVE, NEVADA

Open-File Report 83-377

1983

This report is preliminary and has not been reviewed for conformity with U.S. Geological Survey editorial standards and stratigraphic nomenclature. Company names are for descriptive purposes only and do not constitute endorsement by the U.S. Geological Survey.

Prepared by the U.S. Geological Survey
for the
U.S. Department of Energy
(Interagency Agreement DE-AI08-76DP00474)
and the
Defense Nuclear Agency

Copies of this Open-file Report
may be purchased from

Open-File Services Section
Branch of Distribution
U.S. Geological Survey
Box 25425, Federal Center
Denver, Colorado 80225

PREPAYMENT IS REQUIRED

Price information will be published
in the monthly listing
"New Publications of the Geological Survey"

FOR ADDITIONAL INFORMATION
CALL: Commercial: (303)234-5888
FTS: 234-5888

United States
Department of the Interior
Geological Survey

GEOLOGIC AND GEOPHYSICAL INVESTIGATIONS OF CLIMAX STOCK INTRUSIVE, NEVADA

by

U. S. Geological Survey

Chapter A--Geologic Investigations
by Paul P. Orkild[1], D. R. Townsend[2], and M. J. Baldwin[2]

Chapter B--Gravity Investigations
by D. L. Healey[1]

Chapter C--Magnetic Investigations
by G. D. Bath[1], C. E. Jahren[1], J. G. Rosenbaum[1], and M. J. Baldwin

Chapter D--Summary of Geologic and Geophysical Investigations by Paul P. Orkild

[1] U.S. Geological Survey, Denver, Colo.

[2] Fenix & Scisson, Inc., Mercury, Nev.

FOREWORD

Successful detection of underground nuclear detonations requires investigation of the effects of seismic discontinuities near large geologic features. As part of the Defense Nuclear Agency seismic testing program, the U.S. Geological Survey was requested to define the extent of buried intrusive rock at the Climax stock in the northeastern part of the Nevada Test Site, and to define the nature of geologic contacts with adjoining rock units.

Geologic data were used to define the surface structure in the area of proposed emplacement holes for the nuclear seismic test, code named Midnight Blue. Geologic and geophysical data define the geometry of the stock and other geologic features pertinent to containment of the nuclear test.

Chapter A, GEOLOGIC INVESTIGATIONS
by Paul P. Orkild, D. R. Townsend, M. J. Baldwin

CONTENTS

ILLUSTRATIONS

TABLES

Chapter B, GRAVITY INVESTIGATIONS
By D. L. Healey

CONTENTS

ILLUSTRATIONS

Chapter C, MAGNETIC INVESTIGATIONS

by G. D. Bath, C. E. Jahren, J. G. Rosenbaum, and M. J. Baldwin

CONTENTS

ILLUSTRATIONS

ILLUSTRATIONS--Continued

TABLES

ILLUSTRATIONS

MAGNETIC INVESTIGATIONS

G. D. Bath, C. E. Jahren, J. G. Rosenbaum, and M. J. Baldwin

ABSTRACT

Air and ground magnetic anomalies in the Climax stock area of the NTS help define the gross configuration of the stock and detailed configuration of magnetized rocks at the Boundary and Tippinip faults that border the stock. Magnetizations of geologic units were evaluated by measurements of magnetic properties of drill core, minimum estimates of magnetizations from ground magnetic anomalies for near surface rocks, and comparisons of measured anomalies with anomalies computed by a three-dimensional forward program. Alluvial deposits and most sedimentary rocks are nonmagnetic, but drill core measurements reveal large and irregular changes in magnetization for some quartzites and marbles. The magnetizations of quartz monzonite and granodiorite near the stock surface are weak, about 0.15 A/m, and increase at a rate of 0.00196 A/m/m to 1.55 A/m, at depths greater than 700 m (2,300 ft). The volcanic rocks of the area are weakly magnetized. Aeromagnetic anomalies 850 m (2,800 ft) above the stock are explained by a model consisting of five vertical prisms. Prisms 1, 2, and 3 represent the near surface outline of the stock, prism 4 is one of the models developed by Whitehill (1973), and prism 5 is modified from the model developed by Allingham and Zietz (1962). Most of the anomaly comes from unsampled and strongly-magnetized deep sources that could be either granite or metamorphosed sedimentary rocks. A combination of horizontal and vertical prisms was used to relate details of structure at faults to ground magnetic anomalies 1.5 m (5 ft) above the surface. The stock is defined at its southeastern edge by the Boundary fault which has dips of 70 to 80° to the southeast and a displacement of 2,000 m (6,500 ft). The western edge of the stock dips at an angle of 30°, and there is no evidence of displaced granitic rock at the Tippinip fault. A small anomaly west of the fault arises from magnetized sedimentary rocks, and not from displaced granitic rocks. New data from a recent aeromagnetic survey show that the trend of positive magnetic anomalies over the Gold Meadows, Climax, and Twinridge stocks extends to the southeast for more than 65 km (40 miles).

INTRODUCTION

This study is similar to several the USGS has undertaken at the NTS and nearby areas to locate large bodies of buried granitic rock, estimate their depths and shapes, and thus define prospects for further investigations as possible sites for storage of radioactive waste. Measurements of magnetic properties indicate that the total magnetization of a granitic mass usually has a normal polarity in the approximate direction of the Earth's magnetic field, and prominent positive anomalies are often found over large exposures of granitic rock. Examples of normally-magnetized quartz monzonite and granodiorite bodies that produce broad positive anomalies include the Climax stock (Allingham and Zietz, 1962), and satellitic stocks or certain plutons within the Sierra Nevada batholith 250 km (155 mi) to the west (Currie and others, 1963; Gromme and Merrill, 1965; and Oliver, 1977). In the test site region metamorphosed sedimentary rocks, volcanic ash, and rhyolitic lava flows may also be magnetized along the Earth's field. They can occur in large volumes and may cause prominent positive anomalies. Identification of a buried source is thus often difficult.

Within the NTS and nearby areas, a number of positive anomalies are positioned over the relatively few intrusive rocks that have been identified during surface mapping and drill-hole logging. The residual aeromagnetic map of figure 1C shows nine magnetic highs that are associated with areas of known intrusive rock, as indicated by letters A through I. Five of the nine areas of intrusive rock are alined across the northern part of the NTS: (A) Twinridge (Barnes and others, 1965); (B) Climax stock (Houser and Poole, 1960, and Barnes and others, 1963): (C) Gold Meadows stock (Gibbons and others, 1963; (D) northwest Pahute Mesa (Orkild and Jenkins, written commun., 1978); and (E) Black Mountain (Noble and Christiansen, 1968). The remaining four areas are (F) Wahmonie (Ekren and Sargent, 1965); (G) Calico Hills (McKay and Williams, 1964); (H) Timber Mountain (Carr and Quinlivan, 1966); and (I) Quartzite Mountain (Rodgers and others, 1967).

Residual maps were prepared by subtracting the regional field from observed anomalies, a process designed to give a residual datum of about zero over large areas underlain by thick deposits of nonmagnetic alluvium and bedrock. To prepare figure 1C, a least-square procedure was applied to data at 3-km grid intervals to define a planar regional field for an area of 10,000 Km^2 (3,860 mi^2) covered by 14 published aeromagnetic maps that includes the NTS and most of the Nellis Air Force Bombing and Gunnery Range: Boynton and Vargo, 1963a,b; Boynton and others, 1963a,b; and Philbin and White, 1965a-j. A graphical method was then used to remove regional from observed contours.

Most anomalies in the stock region appear to be related to outcrops of granitic or volcanic rocks as indicated by comparing positions of the more detailed aeromagnetic anomalies of figure 2C and the generalized geology of plate 1A. The western third of figure 2C was compiled from the survey data of figure 1C, and the eastern two thirds of figure 2C were taken from the survey data of figure 3C. The aeromagnetic survey and compilation of figure 3C were made in 1980 by the U.S. Naval Oceanographic Office for an area of about 3,800km^2 (1,450 mi^2) in eastern Nye and western Lincoln counties, Nevada. This coverage was not available during the compilation of aeromagnetic maps of Nevada by Zietz and others (1977), and Sweeney and others (1978).

Some of the significant aeromagnetic anomalies of figure 2C have been investigated in recent years and their sources can be stated with confidence, but others have not and their sources must be inferred. From east to west in figure 2C, the positive anomalies arise from the following sources: an inferred stock that is covered by older sedimentary rocks at A in the Papoose Range; a quartz monzonite stock that is mostly covered by alluvium, volcanic rock, and older sedimentary rock at B near Twinridge hill; a body of quartz monzonite and granodiorite C at Climax stock; an inferred stock that is covered by volcanic rock at D northwest of Climax stock; and a body of quartz monzonite E at Gold Meadows stock.

The strongly-magnetized volcanic rocks in the Climax region have reversed magnetic polarities and produce negative anomalies. From east to west in figure 2C, negative anomalies arise from the following sources: the Rainier Mesa Member ash flow (Sargent and Orkild, 1973) at Aqueduct Mesa F and at Rainier Mesa G; and from pre-Ammonia Tanks rhyolite lavas (Byers and others, 1976) buried by alluvium and volcanic flows at H, I, and J in the Timber Mountain caldera, and exposed and penetrated by drilling at K on Pahute Mesa.

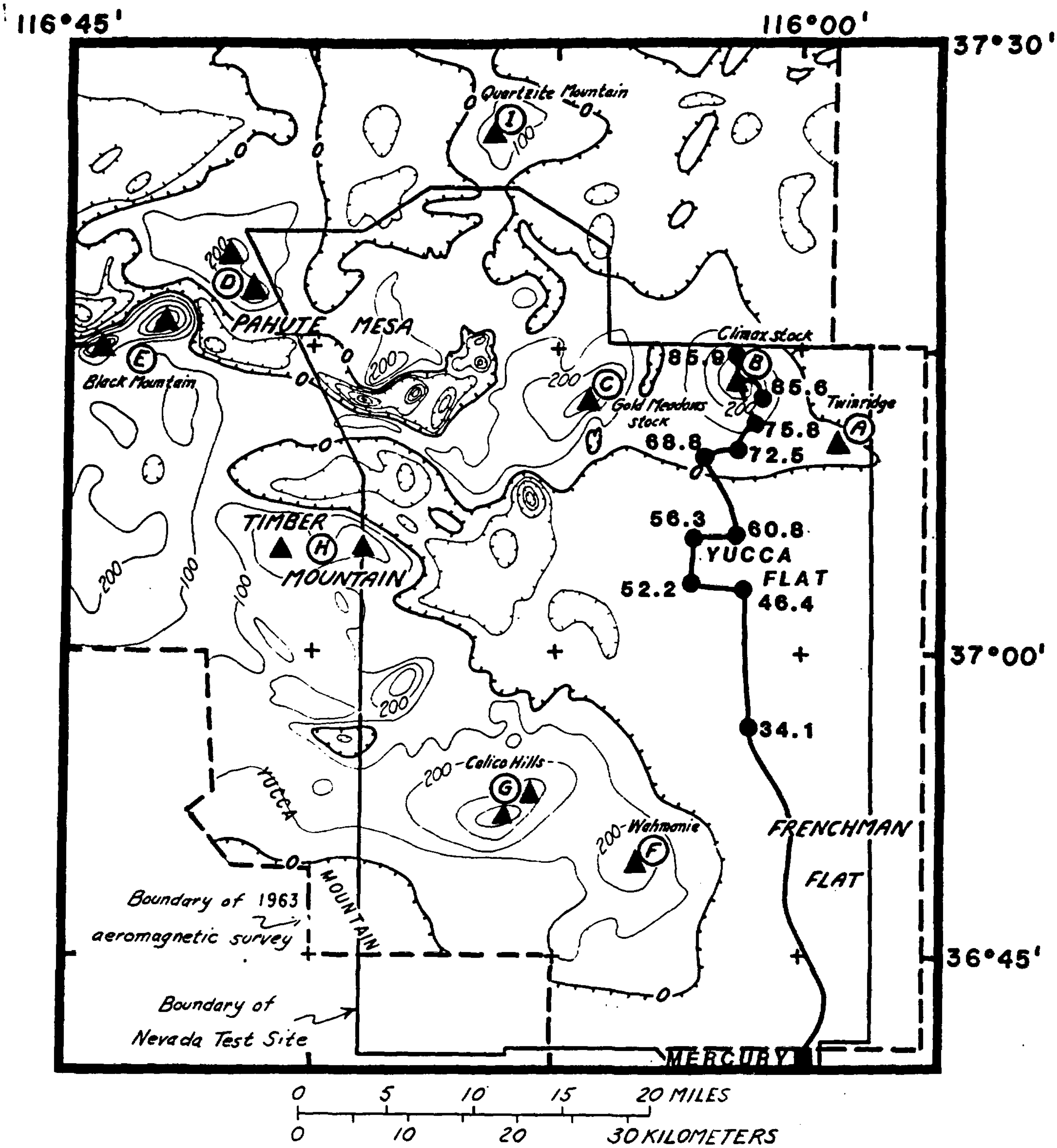

Figure 1C--Residual aeromagnetic map of Nevada Test Site and nearby regions showing nine prominent positive anomalies (lettered A through I), over exposed granitic rock, or over areas where granitic rock is inferred at depth. Measurements were at about 2,450 m (8,000 ft) above sea level, contour interval is 100 nanoteslas, and zero and negative contours are hachured. The bold hashured line represents the zero contour that separates positive from negative residual anomalies. Solid triangles give locations of anomaly maxima, and solid line indicates traverse along which ground magnetic anomalies were measured by a truck-mounted magnetometer from Mercury to Climax stock. Traverse distances are in kilometers.

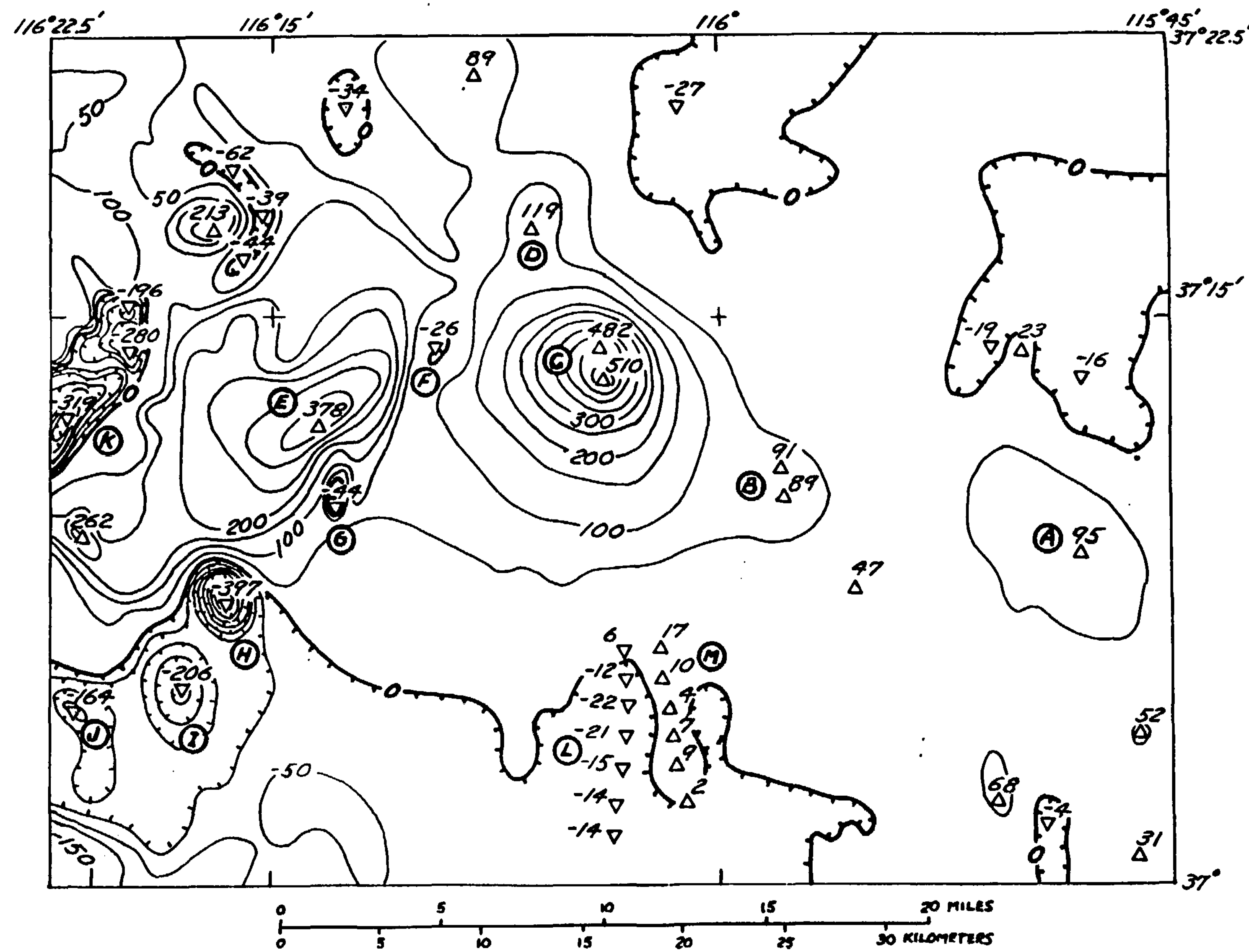

Figure 2C.--Residual aeromagnetic map of Climax stock region showing broad positive anomalies (lettered A through E), over known or inferred granitic rock; narrow negative anomalies (lettered F through K), over known or inferred volcanic rock; and anomaly minima (near L) and maxima (near M), over volcanic rock along the Yucca fault. Measurements were at about 2,480 m (8,000 ft) above sea level for western third of map, and at about 2,130 m (7,000 ft) for eastern two thirds of map. Contour interval is 50 nT, and zero and negative contours are hachured. Triangles give locations of anomaly maxima, and inverted triangles give locations of anomaly minima.

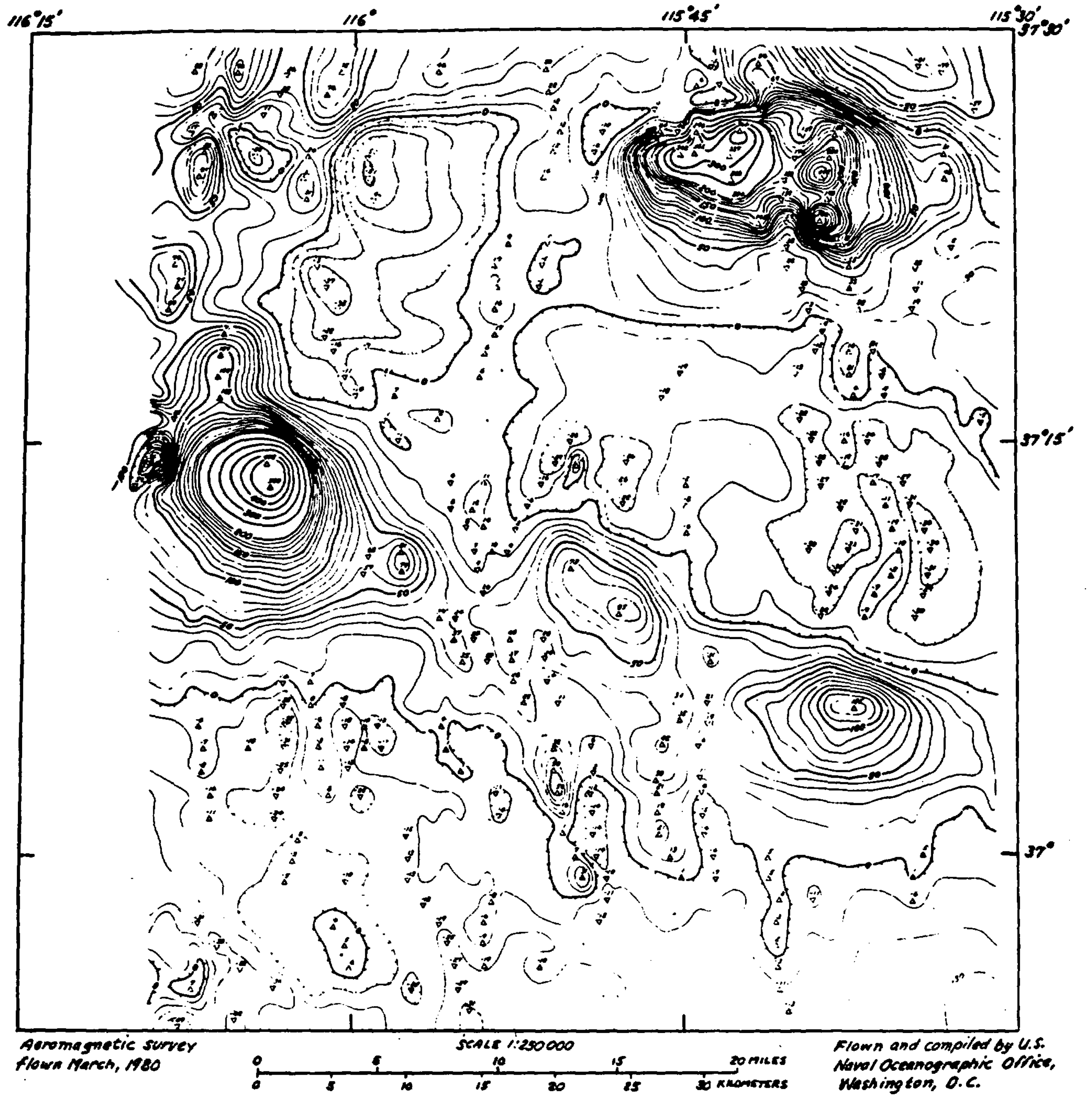

Figure 3C.--Aeromagnetic map of parts of eastern Nye and western Lincoln Counties, Nevada, showing residual anomalies in total magnetic intensity relative to 1980 International Geomagnetic Reference Field. Datum was increased 280 nT to give values near zero over large areas of nonmagnetic rock. Contour intervals are 10 and 50 nT, and zero and negative contours are hachured. Triangles give locations of anomaly maxima, and inverted triangles give locations of anomaly minima. Measurements were at about 2,285 m (7,500 ft) barometric elevation for southern half and about 2,560 m (8,400 ft) for northern half of map.

Also, the Rainier Mesa Member ash flow, which underlies alluvium and a volcanic flow along the Yucca fault, produces a line of negative anomalies L on the high-standing side of the fault, and a positive anomalies M on the low-standing side of the fault.

MAGNETIC PROPERTIES

The average total magnetization of a uniformly magnetized rock mass, denoted as the vector $\vec{J}_t$, is defined as the vector sum of the induced magnetization, $\vec{J}_i$, and remanent magnetization, $\vec{J}_r$:

$$\vec{J}_t = \vec{J}_i + \vec{J}_r.$$

The direction and intensity of induced magnetization is a function of the magnetic susceptibility, k, and field, $\vec{B}_0$:

$$\vec{J}_i = \frac{kB_0}{\mu_0},$$

where $\mu_0 = 4\pi x 10^{-7}$ henrys/m.

Remanent magnetization, on the other hand, is independent of the external field. The Koenigsberger ratio (1938), $Q = J_r/J_i$, is often used to indicate the relative contribution of the two components to J_t.

Air and ground magnetic surveys will usually detect a geologic unit when its total magnetization is equal to or greater than 0.05 A/m (ampere per meter). Therefore, rocks having average intensities less than 0.05 A/m are designated nonmagnetic; and those having greater intensities are here arbitrarily designated as either weakly, moderately, or strongly magnetized, as defined by the following limits:

nonmagnetic < 0.05 A/m
0.05 A/m < weakly magnetized < 0.50 A/m
0.50 A/m < moderately magnetized < 1.50 A/m
1.50 A/m < strongly magnetized

The magnetic properties of older sedimentary rocks, granitic rocks, volcanic rocks, and alluvial deposits in the Climax region were estimated by collecting and measuring surface and drill core samples, and by relating maximum slopes of ground magnetic anomalies to minimum estimates of magnetization for geologic features close to the surface. Also, general information is available on the magnetic properties of NTS rocks of nearby areas (Bath, 1968, 1976).

Estimate of Magnetization

A minimum estimate of total magnetization, J_t, is given by Smith (1961, equation 2.7) which requires information only on anomaly amplitude and depth to the magnetized body. No assumptions are necessary for body shape or direction of magnetization except that the direction must be uniform throughout the body. The anomaly amplitude, t, is measured between two points separated by a distance, c. The relation is given by

$$J_t \geq \hat{J}_t = \frac{|t|}{F\left(\frac{h}{c}\right)} \tag{1}$$

where h is the depth to anomaly source, and $F\left(\frac{h}{c}\right)$ is a function tabulated by Smith.

In our studies, the anomaly amplitude is measured over the slope distance, c, as defined by Vacquier and others, 1951. The distance is designated the maximum slope parameter by Nettleton (1976 p. 395-403), and it is commonly assumed equal to the approximate depths of anomaly-producing bodies. Under this assumption, c = h, and equation 1 reduces to a simple expression,

$$\hat{J}_t = \frac{|t|}{289} \tag{2}$$

when J_t is expressed in A/m, and t in nanoteslas.

The amplitudes of ground magnetic anomalies can now be employed to designate magnetizations of near surface rocks as follows:

nonmagnetic < 15 nT
15 nT < weakly magnetized < 150 nT
150 nT < moderately magnetized < 450 nT
450 nT < strongly magnetized

Ground magnetic surveys have been used as a convenient and prompt method over large areas of the Test Site and have provided estimates of magnetization for geologic features at or near the surface that compare favorably with magnetic properties determined from surface and drill-core samples in the laboratory. For example, the anomaly profile of traverse B66-B66', located on the west side of the stock (fig. 4C), indicates dolomite and marble are nonmagnetic, and that masses of quartz monzonite within 10 m (32.8 ft) of the surface are only weakly magnetized (fig. 5C). Slope distances and their respective t and c components are shown along the traverse for the three strongest anomalies on the traverse which occur over the quartz monzonite. The amplitudes average 75 nT and yield a minimum estimate for J_t of 0.26 A/m. Elsewhere on the traverse the amplitudes are considerably less, but remain mostly within the weakly-magnetized range.

Older Sedimentary Rocks

Sedimentary rocks of Paleozoic and Precambrian age at the NTS consist mainly of argillite, dolomite, limestone, and quartzite that are usually found to be nonmagnetic. Thick deposits are often present within large areas characterized by a relatively uniform aeromagnetic field. This is illustrated by the thick section of quartzite and marble of the Eleana Formation in the Eleana Range west of Yucca Flat on plate 1A, and the lack of a significant magnetic anomaly over the Eleana Range in the aeromagnetic map of figure 2C. There are, however, notable exceptions to this generalization, as observed in

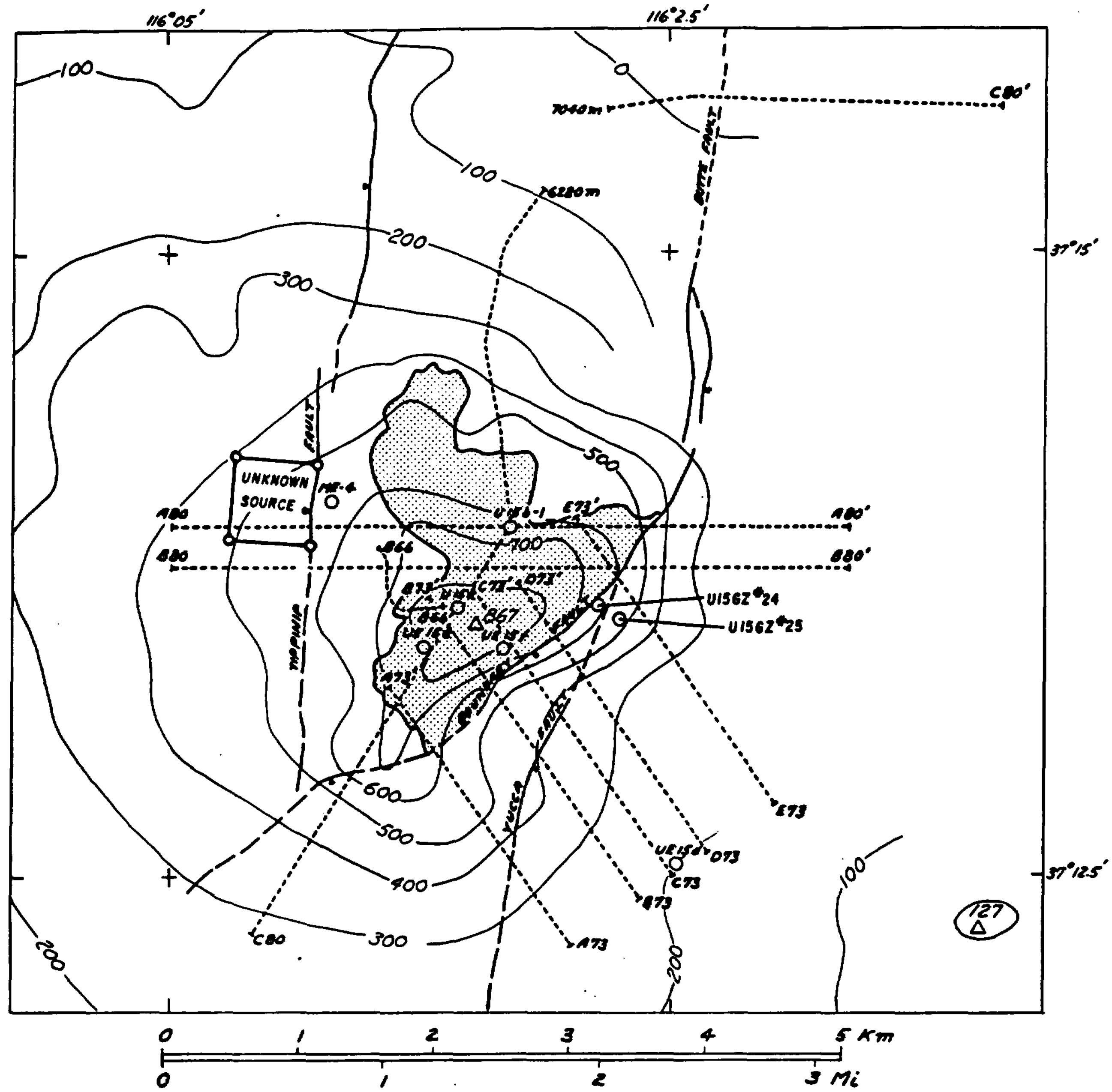

Figure 4C.--Residual aeromagnetic map showing broad positive anomaly over Climax stock (shaded outline of exposed part of stock); major faults bordering the stock; drill holes ME-4, U15b-1, U15a, UE15e, UE15f, U15gz#24, U15gz#25, and UE15d; ground traverses A80-A80', B80-B80', C80-C80', A73-A73', B73-B73', C73-C73', D73-D73', E73-E73', and B66-B66'. Square outline of unknown source was used on figure 20 to model Tippinip fault. Measurements were at about 120 m (394 ft) above the ground surface; contour interval is 100 nT, and triangles give locations of anomaly maxima. Readings were not taken along interval 6,280 to 7,040 m (20,604-23,097 ft) over steep topography of ground traverse C80-C80'.

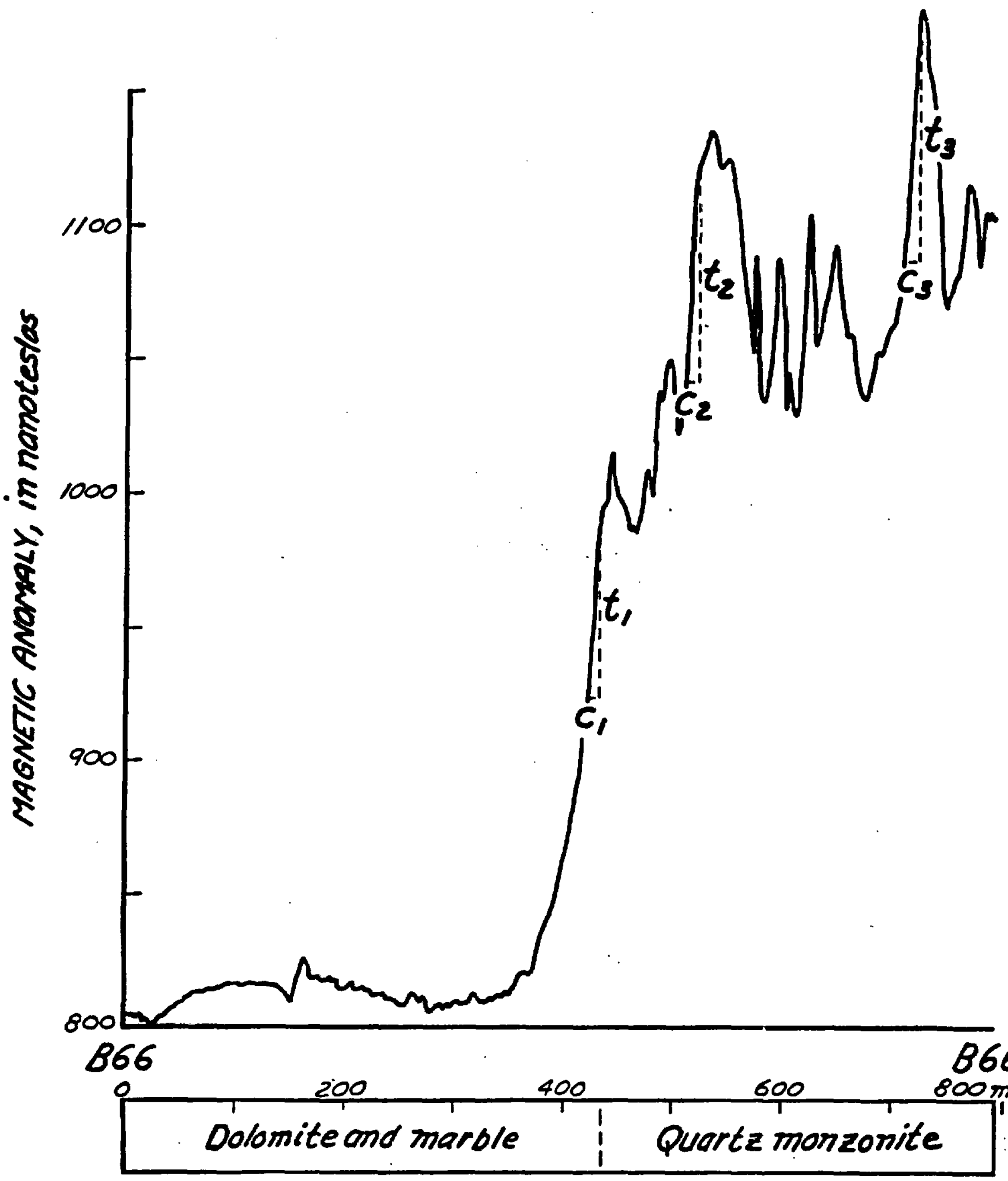

Figure 5C.--Profile of residual ground magnetic anomalies along traverse B66-B66' over dolomite and marble, and quartz monzonite showing distances, c and amplitudes, t, that are used to compute minimum estimates of magnetization. Profile is plotted from 516 rubidium magnetometer measurements 1.5 m (5 ft) above ground surface.

the magnetic properties of surface exposures and drill core from the Calico Hills (Baldwin and Jahren, 1982), and in the core from two holes drilled near the Climax stock. At Calico Hills in the southwestern part of the NTS, the strongly-magnetized argillite of the Eleana Formation appears to be the principal cause of the prominent aeromagnetic anomaly, G of figure 1C. In that region, nonmagnetic argillite has been altered to strongly-magnetized rock, apparently by the conversion of pyrite to magnetite. At the Climax stock, similar high values of magnetic susceptibility were reported by P. H. Cole and W. P. Williams (written commun., 1962) for a 200 m (656 ft) interval of quartzite and siltstone in drill hole UE15d.

Measurements of susceptibility and remanent intensity of core samples from drill holes UE15d and ME-4 fig. 4C supplement the magnetic property data mentioned above. UE15d penetrated 88 m (289 ft) of alluvium, 452 m (1,483 ft) of gently dipping volcanic rocks, and 1,288 m (4,226 ft) of steeply dipping Precambrian metasedimentary rocks (Harley Barnes, written commun., 1962). ME-4 penetrated 350 m (1,148 ft) of marble and 5 m (16 ft) of granite.

Magnetic susceptibilities of core samples were measured by means of a digital susceptibility meter which is available commercially; and induced magnetizations were computed from susceptibilities using the formula

$$J_i = (k_{SI}/4\pi)\ B_{nT} x 10^{-2}, \text{ where } B_{nT} = 51900 \text{ nT},$$

the strength of the Earth's field in the stock area. Susceptibilities and remanent magnetizations of representative samples were then determined by the method of Jahren and Bath (1967). Koenigsberger ratios were computed from these measurements and average values were assigned to the various rock types. Total magnetizations were computed for all samples by assuming a normal polarity of remanence, and by using the relation

$$J_t = (Q + 1)\ J_i.$$

Averages of total magnetization vary from nonmagnetic to moderately magnetic for older sedimentary rocks available from the two drill holes, as shown in tables 1C and 2C. Values of Q were based on only 42 samples. The Q values used in the tables, their standard deviations, and the number of samples are 0.5±1.0 for 10 samples of quartzite, 2.0±1.9 for 12 samples of marble, 0.3±0.3 for 5 samples of granite, and 0.9±1.7 for 15 samples of volcanic rock.

A reliable estimate of the magnitude of magnetization for the sedimentary sequence penetrated by drilling could not be determined because of large, apparently unsystematic changes in total magnetization from nonmagnetic to 9.59 A/m in UE15d and 5.81 A/m in ME-4, and insufficient available core. No consistent pattern of magnetization could be determined. The values do not increase with depth, or with relation to known granitic rock at ME-4, or to inferred granitic rock at UE15d. Samples from two zones, 1168-1354 m (3,832-4,442 ft) in UE15d and 335-338 m (1,099-1009 ft) in ME-4 have average total magnetizations of 0.7 A/m and 1.4 A/m respectively (tables 1C and 2C). This result indicates that both the quartzite and the marble may show moderate magnetizations comparable to that of granite. If present in sufficient thicknesses, these magnetized sediments will contribute to the aeromagnetic anomaly, and their effects may be indistinguishable from those of the intrusive.

Table 1C.--Average induced magnetization, J_i, and total magnetization, J_t, of core of irregular shape from drill hole UE15d.

Rock type	Interval sampled: Depth (m)	Thickness (m)	Core available (m)	Number of samples	J_i (A/m)	Assigned Q	J_t (A/m)
Volcanic tuff	228-541	313	295	15	0.16	0.9	0.3
Quartzite	541-1,140	599	285	(1/)	<.05	.5	<.1
Quartzite	1,140-1,168	28	7	25	.08	.5	.1
Quartzite	1,168-1,354	186	35	291	.49	.5	.7
Quartzite	1,354-1,470	116	30	109	.04	.5	.1
Quartzite	1,470-1,615	145	20	(1/)	<.05	.5	<.1
Dolomite	1,615-1,829	214	35	(1/)	<.05	2.0	<.2

1/ Core scanned with digital magnetic susceptibility meter.

Table 2C.--Average induced magnetization, J_i, and total magnetization, J_t, of core of irregular shape from drill hole ME-4.

Rock type	Interval sampled: Depth (m)	Thickness (m)	Number of samples	J_i (A/m)	Assigned Q	J_t (A/m)
Marble	4-266	262	(1/)	<0.05	2.0	<0.2
Marble	266-278	12	105	.10	2.0	.3
Marble	278-293	15	170	.03	2.0	.1
Marble	293-335	42	(1/)	<.05	2.0	<.2
Marble	335-338	3	32	.46	2.0	1.4
Marble	338-357	19	137	.06	2.0	.2
Granite	357-362	5	33	.52	.3	.7

1/ Core scanned with digital magnetic susceptibility meter.

Granitic Rocks

Large changes in total magnetization, varying from nonmagnetic to strongly magnetic, also were found in 676 core samples of quartz monzonite and granodiorite. Almost continuous core was available from four holes shown on figure 4C: U15a drilled to 366 m (1,201 ft) depth in moderately-magnetized quartz monzonite and strongly-magnetized granodiorite, U15b-1 drilled to 549 m (1,801 ft) depth in moderately-magnetized granodiorite, UE15e drilled horizontally for a distance of 183 m (600 ft) into the side of a hill of weakly-magnetized quartz monzonite, and UE15f drilled to 100 m (328 ft) depth in moderately-magnetized quartz monzonite. Average magnetic properties are given in table 3C. Sample volumes were included to indicate sample size, and thus, the type of instrument used for measurements. Measurements on large drill core samples were made with equipment described by Jahren and Bath (1967). For small cores, magnetic susceptibilities were measured with a device similar to that described by Christie and Symons (1969) and calibrated by the method of Rosenbaum and others, 1979. Remanent magnetizations were measured with a spinner magnetometer which is commercially available.

Table 3C.--Average sample volume, induced magnetization, J_i, Koenigsberger ratio, Q, and total magnetization, J_t, of 676 core samples of cylindrical shape from drill holes U15a, U15e, U15f, and U15b-1.

				Average			
Rock type	Drill hole	Interval sampled (m)	Number of samples	Sample volume1/ (cm^3)	J_i (A/m)	Q	J_t (A/m)
Quartz monzonite	U15a	122	5	13	0.76	(2/)	0.84
Quartz monzonite	UE15e	181	121	310	.09	(2/)	.10
Quartz monzonite	UE15f	187	124	425	.67	(2/)	.74
Granodiorite	U15a	244	19	13	1.53	(2/)	1.68
Granodiorite	U15b-1	533	351	535	.67	0.22	.82
Granodiorite	U15b-1	533	56	13	.87	.08	.94

1/ Sample volumes greater than 300 cm^3 indicate pieces of actual drill core sawed to cylinders having lengths about equal to diameters. Samples of 13-cm^3 volume were obtained by drilling 2.54-cm diameter cores from the drill core, and sawing ends off to give about 2.54-cm lengths.

2/ J_r not measured; assume Q = 0.10.

The magnetic properties of drill core indicate magnetizations increase with depth in the quartz monzonite and granodiorite stocks. Allingham and Zietz (1962) report the upper 122 m (400 ft) of quartz monzonite from drill hole U15a is moderately magnetized and the lower 244 m (800 ft) of grandiorite is strongly magnetized. Quartz monzonite from the horizontal hole, UE15e, is within 90 m (295 ft) of the surface and weakly magnetized, while quartz monzonite from the vertical hole, UE15f, is within 187 m (614 ft) of the surface and moderately magnetized. Hole U15b-1 extends to a greater depth, 533 m (1,749 ft) in granodiorite, and it was selected to provide the magnetization data that were used in computing a model for this report. About 350 large samples, averaging 535 cm^3, were collected at approximately 1.5-m (5-ft) intervals. A total of 56 small samples, approximately 13 cm^3 in volume, were collected with groups of 2 to 4 specimens separated by approximately 30 m (98 ft). Average induced magnetizations and Koenigsberger ratios are given in table 3C for the large and small samples, and individual values of induced magnetization for the large samples are plotted versus depth in figure 6C.

The line shown in figure 6C is the result of linear regression having a correlation coefficient of 0.75. The line indicates a weak near surface magnetization of 0.13 A/m and an increase of 0.00196 A/m per meter of depth. Linear regression of the small sample data yields similar results with the near surface magnetization being 0.16 A/m and the increase being 0.00225 A/m per meter of depth (correlation coefficient 0.83). Correlation coefficients for higher polynomials are negligibly larger; a fifth order fit to the large sample data produces a correlation coefficient of 0.75.

Remanent magnetization of samples from U15b-1 are low with respect to the induced component with Q averaging less than 0.25 (table 3C). Therefore, the contribution of remanence may be safely ignored for modeling purposes.

Study of opaque minerals in thirteen polished thin sections from U15b-1 indicates that the increase of induced magnetization with depth is due to an increase in the original magnetite content, and not due to deep weathering effects or to changes in size of magnetite grains. The quantity of magnetite observed ranged from 0.1 to 0.65 percent, and a linear regression of percent magnetite versus magnetic susceptibility yielded a correlation coefficient of .81. The magnetite observed in twelve thin sections collected from depths greater than 30 m (98 ft) is largely unaltered. However, the granodiorite in the remaining thin section, from a depth of 13 m (43 ft) is highly altered and approximately 30 percent of the magnetite has been replaced by hematite.

Volcanic Rocks and Alluvial Deposits

Volcanic rocks of Oligocene and Miocene age in the immediate area of the stock consist of bedded, zeolitized, air-fall, and reworked tuffs that generally have weak magnetizations, as well as ash-flow tuffs that generally have weak to moderate magnetizations. Bath (1968) reported that induced magnetizations of most volcanic units in the Test Site area are weak, and it is the strong remanent magnetizations of welded ash flows and lava flows that are responsible for many prominent aeromagnetic anomalies. No strongly-magnetized ash or lava flows occur over or near the Climax stock.

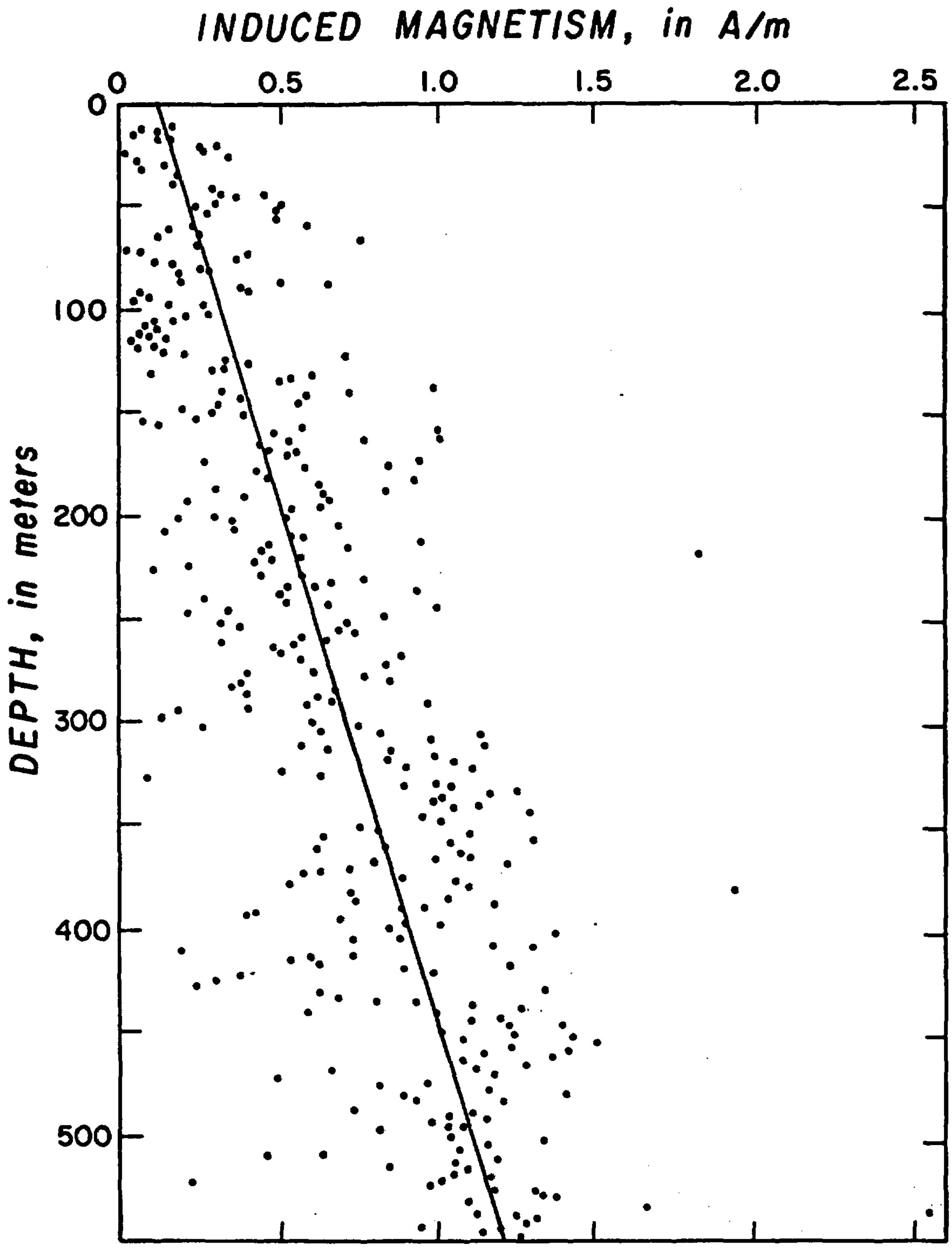

Figure 6C.--Induced magnetization of 351 large core samples of granodiorite with fitted line of linear regression showing an increase in magnetization of 1.05 A/m for a depth interval of 533 m (1,750 ft) in drill hole U15b-1.

Alluvial deposits of Holocene age consist of fragments of reworked granitic, volcanic, and sedimentary rocks. The heterogenous and haphazard manner of deposition results in cancellation of most of the contribution of remanent magnetization. Total magnetizations of alluvium are therefore almost entirely induced magnetizations that are generally categorized as nonmagnetic.

Minimum estimates of magnetization from ground magnetic anomalies indicates most near surface features in the stock area can be designated as either nonmagnetic or weakly magnetized. A 2,100-m (6,900-ft) traverse mostly over alluvium on the southeastern side of the stock illustrates the ambient level of anomaly response that is expected over nonmagnetic rock. Figure 7C shows anomalies measured 1.5 m (5 ft) above the surface along the 80.5 to 82.6 km (50 to 51.3 mi) portion of the long traverse of figure 1C. A rubidium magnetometer was carried 30 m (98 ft) behind the truck in order to eliminate magnetic "noise" caused by the truck. Part A of figure 6C shows residual anomalies that are based on a zero datum over Yucca Flat, and include regional effects of the stock and local effects of the alluvium. Part B shows amplified anomalies after regional effects of the stock have been removed. The anomaly at 80.74 km (50.2 mi) arises from weakly magnetized quartz monzonite at the alluvium-stock contact, and the anomaly at 82.44 km (51.2 mi) arises from a metal sign post. All other anomalies are assumed to be produced by alluvium at or near the surface. Almost all anomaly amplitudes over maximum slope distances are less than 15 nT, the division between nonmagnetic and weakly-magnetized rock.

OBSERVED AND RESIDUAL ANOMALIES

The data recorded by a magnetometer during an aeromagnetic or ground magnetic survey consists of the effects of the geologic feature being studied plus the combined effects of the Earth's magnetic field, and all the magnetized geologic features and man-made objects in a large area near the surface or deeply buried. Several methods have been used to identify and separate these components, and Nettleton (1976, p. 134-187) describes anomaly separation and filtering procedures in detail. In order to isolate the anomaly of interest we first define a reference surface, usually referred to as the regional anomaly, to represent effects from the long wavelength anomalies of the Earth's magnetic field and of geologic features buried at great depth. The regional anomaly then becomes the zero datum upon which residual values are based. An ideal residual anomaly map includes only the short wavelength effects of the feature, or features, under study; but in practice extraneous and overlapping effects are present.

We commonly use two methods to determine regional anomalies for aeromagnetic surveys of large areas. In one method, the regional anomaly consists of a planar surface established by a least-squares fit to data at 3-km (1.86-mi) grid intervals. This method was used in deriving figure 1C and produces contour values that are about zero over large areas of thick, nonmagnetic material. In the second method, the regional anomaly is the International Geomagnetic Reference Field (IGRF) and determined by spherical harmonic analysis of worldwide measurements on a 2^{o} grid (Barraclough and Peddie, 1978). In the area of the NTS, this method produces residual values that are about 280 nT lower than the first method. The IGRF was used in compiling figure 3C and 280nT was added to residual values to make the contours consistent with those of figure 1C.

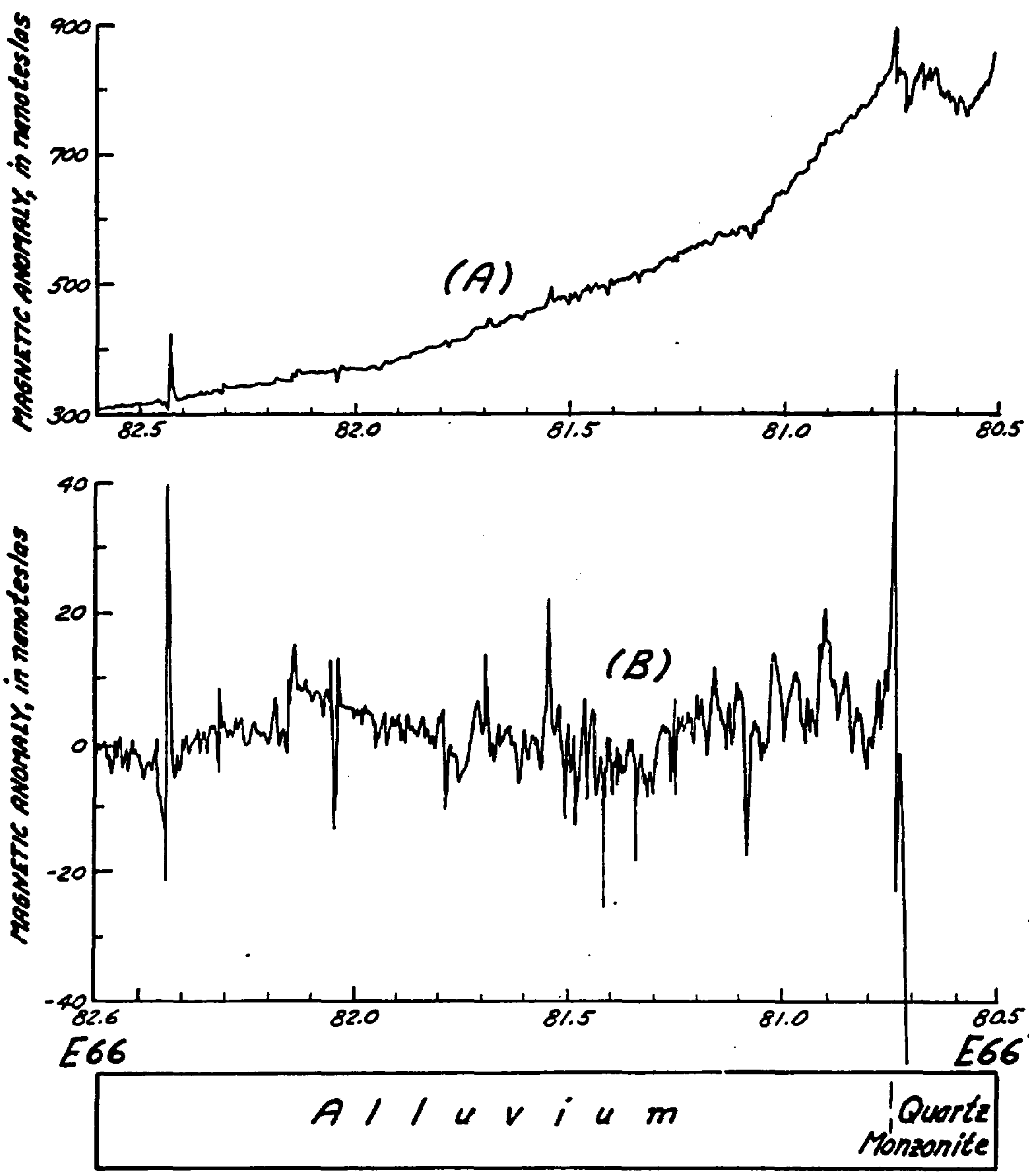

Figure 7C.--Profiles of residual ground magnetic anomalies along the same traverse E66-E66' over alluvium and quartz monzonite showing distances and amplitudes used to compute minimum estimates of magnetization. Profiles are plotted from 1200 rubidium magnetometer measurements 1.5 m (4.9 ft) above ground surface. Profile A is based on zero datum from Yucca Flat, and profile B is based on an average zero datum adjusted to fit the observed data. Distances are in kilometers from Mercury.

For quantitative interpretations of individual anomalies, further adjustment may be required to obtain values closer to zero over nearby deposits of nonmagnetic sedimentary rock. In this report, surfaces are adjusted to an assumed zero field over Yucca Flat where thick deposits of sedimentary rocks underlie relatively thin deposits of alluvium and volcanic rock. For example, a value of 40 nT was added to contours of figure 1C to prepare figure 10C, and 10nT was added to contours of figure 3C to prepare the eastern two thirds of figure 2C.

Measurements were made along a long truck-borne magnetometer traverse to investigate the field over Yucca Flat, and to establish a base station near the Climax stock. The measurement and compilation system was based on work by Kane and others (1971) and Hildenbrand and Sweeney (written commun., 1980). The traverse shown in figure 1C originates at the Mercury base station where investigations during recent years have assigned an Earth's field value of 51550 nT (nanoteslas) and a residual anomaly value of zero. The traverse goes northward on the Mercury highway, along Frenchman Flat, through Yucca Flat, across granitic exposures at Climax stock, and ends at the 85.6-km (53.2-mi) station. Figure 8C shows observed values of the Earth's field along the traverse. The solid line drawn through the anomalies is based on the planar regional anomaly of the NTS region and increases 5.63 nT/km northward and 1.72 nT/km eastward. The line crosses Yucca Flat at about the same average value as the observed anomalies, and at station 75.8 km (47.1 mi) the difference between line and observed value is about 200 nT. The station is therefore assigned a residual value of 200 nT and an Earth's field value of 51880 nT. All ground magnetic traverses measured over the stock were tied to this station.

Figure 9C shows the residual anomalies that result from subtracting regional anomaly values from observed data in part of the profile of figure 8C. The traverse starts at station 34.1 at the south end of Yucca Flat, goes northward across the Flat and stock, and ends at the 85.9 km (53.4 mi) station shown in figure 1C. The residual values were continued upward by the two-dimensional method of Henderson and Zietz (1949) to a level of 2,450 m (8,000 ft) above sea level, the elevation datum of figure 1C. The continuation smoothed and reduced the amplitudes of ground anomalies. Over Yucca Flat the values approach the zero average that has been assumed for both air and ground magnetic anomalies.

REGIONAL INTERPRETATIONS

Recently compiled aeromagnetic data reveal several new anomaly patterns, including a southeastern extension of the belt of positive anomalies that are related to exposures of intrusive rock masses within the NTS. The data are presented on figure 3C at a scale of 1:250,000, the same scale as the geologic map of Lincoln County, Nevada, by Ekren and others (1977).

A trend of positive aeromagnetic anomalies extends from the NTS southeast over known or inferred intrusive bodies for a distance of more than 65 km (40 mi) across eastern Nye and western Lincoln Counties. The anomalies previously shown on figure 2C start at Gold Meadows stock (E) and trend east 20 km (12 mi) to Climax stock (C), southeast 10 km (6 mi) to Twinridge stock (B), and southeast 15 km (9 mi) to the inferred intrusive in the Papoose Range (A).

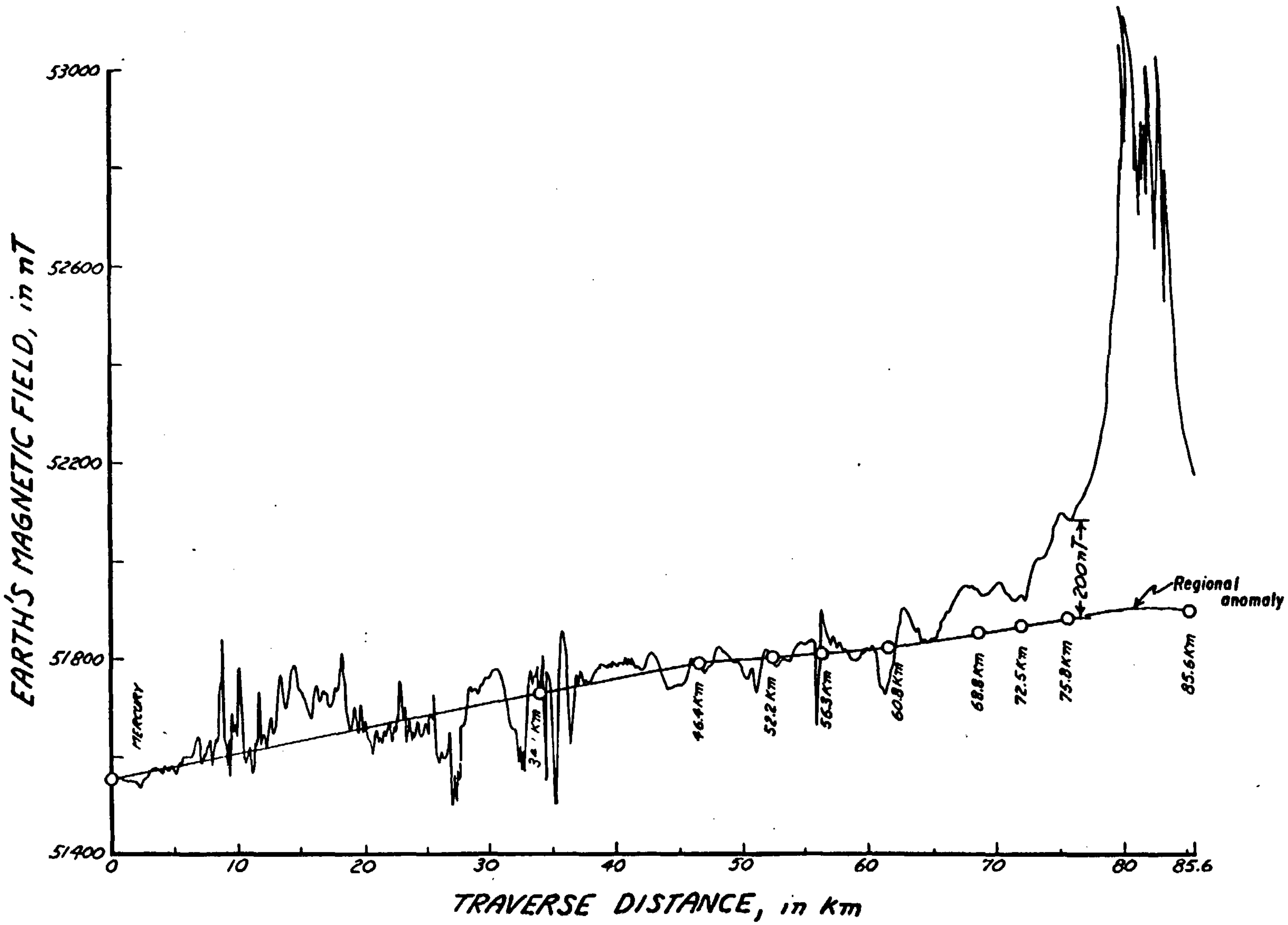

Figure 8C.--Profile of Earth's magnetic field as observed by truck-mounted magnetometer along the traverse of figure 1C extending from base station at Mercury northward 85.6 km (53.2 mi) along west side of Frenchman Flat, 13 to 26 km; through Yucca Flat, 36.6 to 75.8 km; and across granitic exposures at Climax stock, 80 to 83 km. Distances given in figure 1C are shown as circles on the regional line. The profile shows local anomalies arising from geologic features, a gradual northward increase in the Earth's magnetic field, and a line representing the planar regional anomaly of the Test Site region. The residual anomaly, difference between observed and regional anomaly, has a value of 200 nT at the 75.8 km base station.

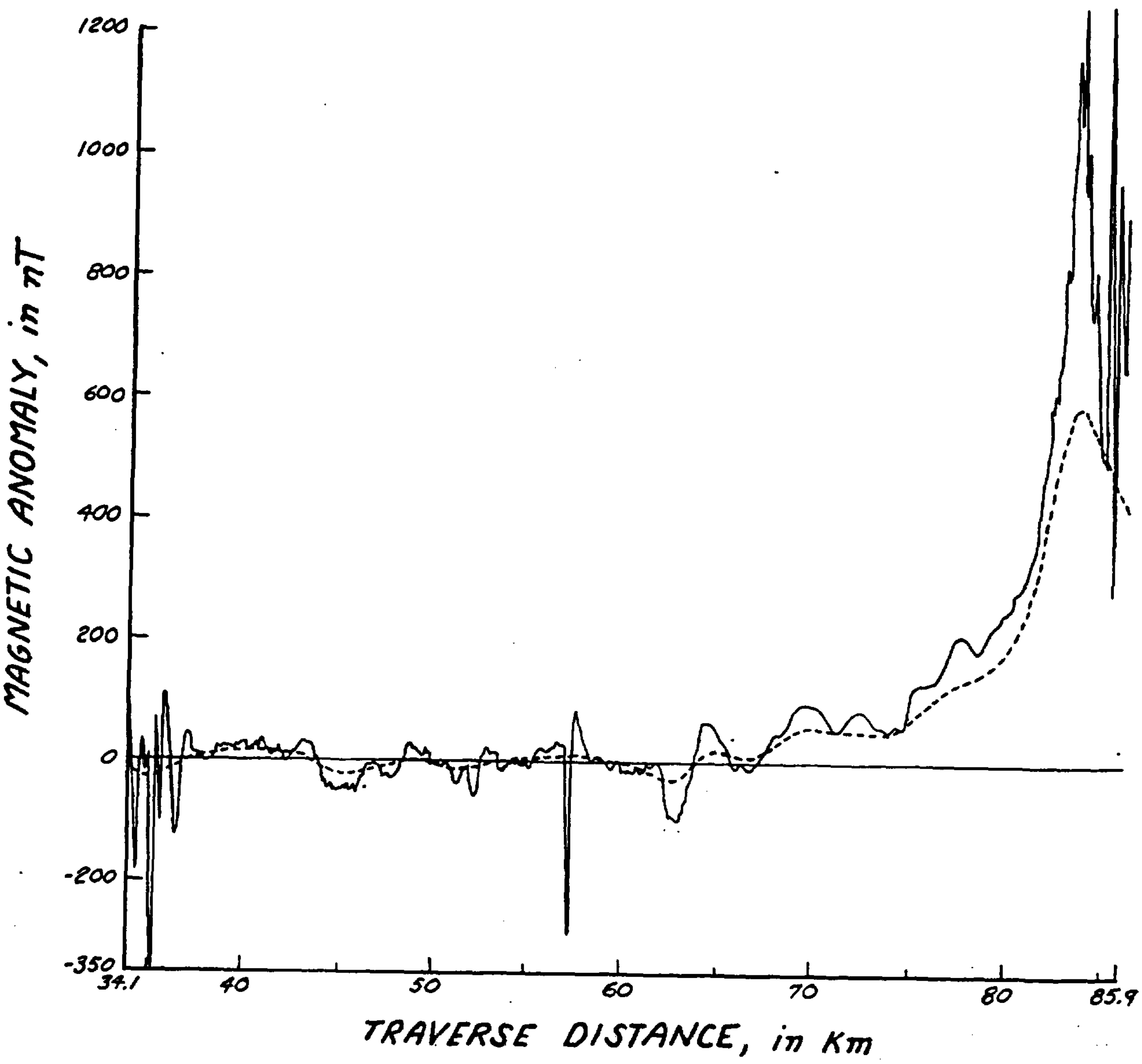

Figure 9C.--Profiles of residual magnetic anomalies, solid line; and data continued upward 914.4 m (3,000 ft), dashed line. Data are from truck-mounted magnetometer traverse of figure 1C extending from 34.1 km (21.2 mi) station northward 51.8 km (32.2 mi) through Yucca Flat, and ending at the 85.9 km (53.4 mi) station on granitic exposures on Climax stock.

The contours of figure 3C extend the trend an additional 20 km (12 mi) southeast to the anomaly maximum of 125 nT over inferred intrusive rock in the northwestern part of the Pintwater Range. The anomalies are interpreted as arising from a belt of magnetized intrusive and associated metamorphosed sedimentary rocks.

The lateral extent of the positive aeromagnetic anomaly in the northeastern corner of figure 4C suggests magnetized intrusives and associated sedimentary rocks are buried beneath the exposures of volcanic rock at the surface. Also, the map shows several belts of alined maxima and minima that strike in a northward direction. The belts are similar to those produced by a faulted volcanic ashflow at the Yucca fault in Yucca Flat (Bath, 1976), and may indicate the presence of buried faults. Data was collected along east-west flight lines, and thus emphasize effects from features that strike north-south.

GROSS CONFIGURATION OF STOCK

Figure 10C is a recompilation of the data of figure 1C at a 20-nT contour interval. The stock anomaly has nearly circular contours over an area of about 200 km^2 (77.3 mi^2), and reaches a maximum of 462 nT at the southwestern edge of the exposed portion of the stock. The compilation is based on measurements 850 m (2,789 ft) above the surface. The effect of the high measurement level is to smooth many of the local anomalies that are found in low-altitude data. Models based on high-altitude data usually represent gross configuration only, and often must be modified in areas where prominent anomalies are present in data measured closer to the ground surface.

Previous Studies

To explain the circular magnetic anomaly, Allingham and Zietz (1962) employed a three-dimensional polar chart method (Henderson, 1960) to produce a model consisting of four cylinders arranged as shown and tabulated on figure 11C. The model represents a gross configuration of the stock that conforms with granitic exposures at the surface, widens and becomes very large at depth, and has steeper slopes on the east and south than to the north and west. The cylinders have a constant magnetization of 1.54 A/m in the direction of the Earth's magnetic field. The magnetization value was determined from core samples in the lower half of drill hole U15a. Figure 11C shows the accepted configuration of the model, and the anomaly that was computed for the model. Subsequently, hole UE15d was drilled to a depth of 1,830 m (6,000 ft) southeast of the stock (fig. 11C). At this location the model of Allingham and Zietz predicts granitic rock at a depth of about 1,400 m (4,600 ft), however, none was encountered in the hole. Possible explanations for failure of the model include (1) the interval of 2,440 m (8,000 ft) from aeromagnetic datum to sea level is too great to give an accurate position for cylinder C, and (2) the granitic rock southeast of the stock is overlain by a thick section of magnetized sedimentary rock.

Whitehill (1973), on the other hand, modeled the circular anomaly with a single rectangular vertical prism. He used a computer to generate anomalies due to a large number of prisims of varying depth, length, width, thickness, and magnetization. Each prism was oriented with its long dimension N. 45° W.

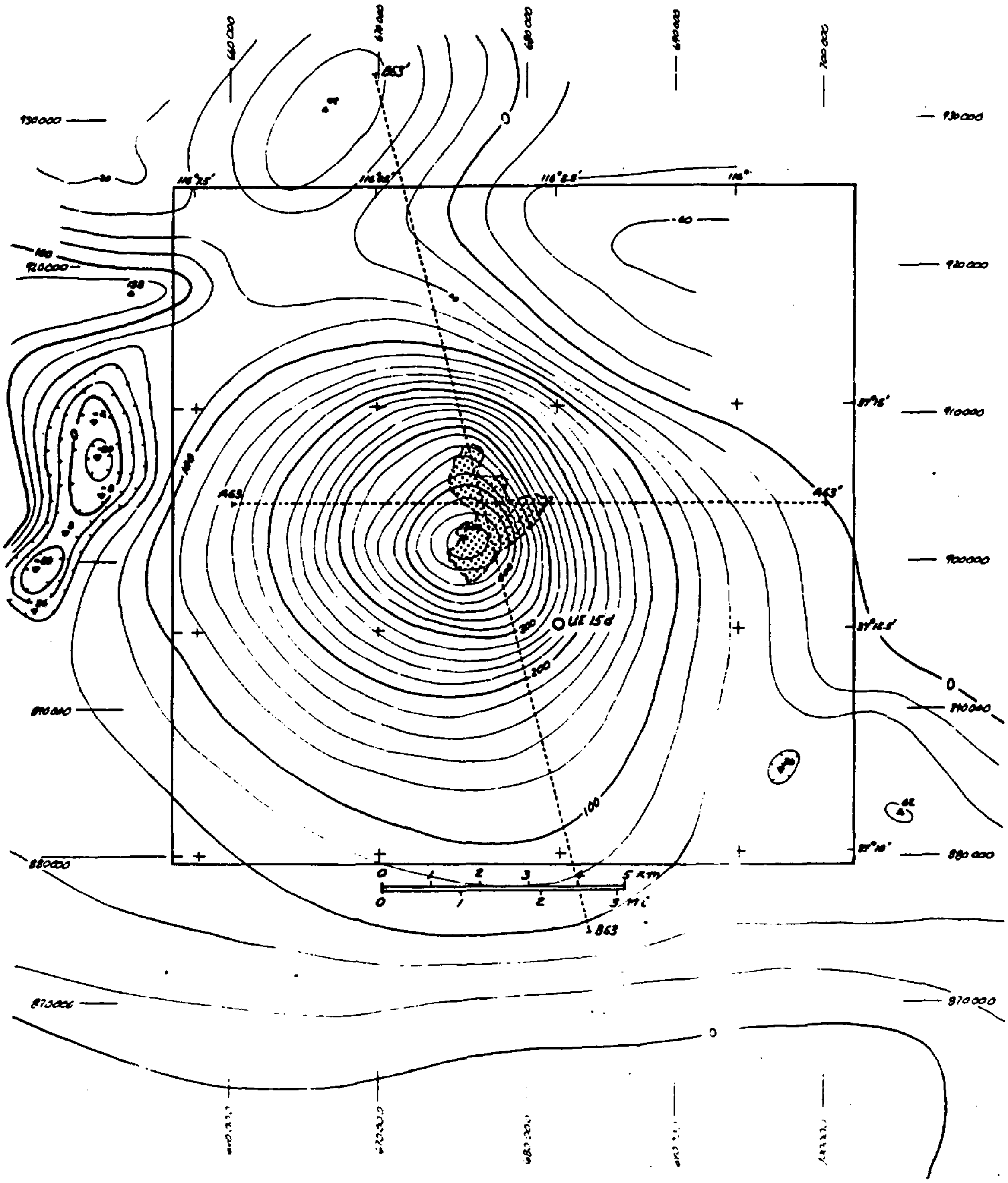

Figure 10C.--Residual aeromagnetic map showing the large circular anomaly that reaches a maximum of 462 nT over shaded outline of exposed part of the stock, and aeromagnetic traverses A63-A63' and B63-B63'. Measurements were at about 2,450 m (8,000 ft) above sea level, and countour interval is 20 nT. Triangles give locations of anomaly maxima, inverted triangles give locations of anamoly minima.

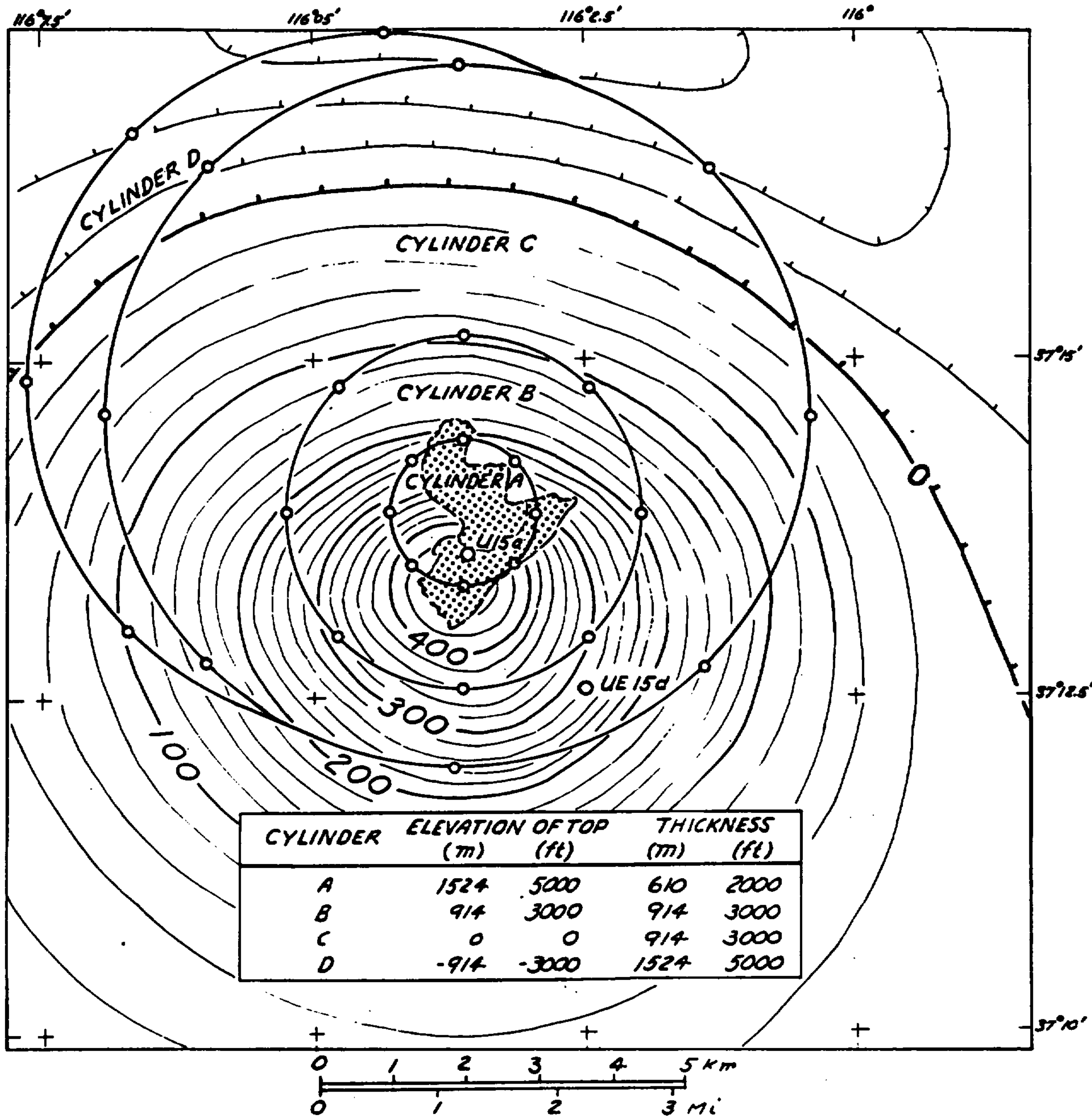

CYLINDER	ELEVATION OF TOP (m)	ELEVATION OF TOP (ft)	THICKNESS (m)	THICKNESS (ft)
A	1524	5000	610	2000
B	914	3000	914	3000
C	0	0	914	3000
D	-914	-3000	1524	5000

Figure 11C.--Outlines and tabulated dimensions of the four vertical cylinders that Allingham and Zietz (1962) used to represent the stock. Also shown and contoured at 20-nT interval is the anomaly computed from four 8-sided vertical prisms arranged to approximate the circular shapes of the four cylinders. Magnetization of all prisms is along the Earth's field at 1.53 A/m, the average intensity of magnetization for core from drill hole U15a. Drill hole UE15d penetrated volcanic and sedimentary rocks to an elevation of -440 m (-1,445 ft), or 440 m below the top of cylinder C, without entering granitic material. Shaded outline is the exposed part of the stock.

The calculated anomalies that best fit the observed anomaly were for prisms that have tops buried beneath the exposed granitic rock at the stock, and magnetizations greater than the 1.54 A/m used by Allingham and Zietz. Figure 12C shows the prism, which provided the best fit to the observed data and its computed magnetic anomaly. The southeast edge of the prisim is 1,220 m (4,000 ft) northwest of drill hole UE15d, its top is 1,173 m (3,850 ft) below granitic rock at the surface, and its magnetization is 2.27 A/m.

New Model of the Climax Stock

We have developed a new model consisting of five vertical prisms to represent the gross configuration of the Climax stock and to explain anomalies along traverses A63-A63' and B63-B63' of figure 10C. The model resulted from considerations that include the locations of granitic exposures, observed increase in magnetization with depth fig. 6C, depths estimated from slope distances of anomalies, and the model of Allingham and Zietz, and of Whitehill. Outlines and dimensions of the new model are shown in plan view on figure 13C and in section along traverse A63-A63' (fig. 13C) on figure 14C. The upper part of the model consists of three 8-sided vertical prisms, P1, P2, and P3, having outlines that closely approximate granitic exposures in plan view. The low surface magnetization of 0.13 A/m increases to 0.28 A/m in P1, 0.72 A/m in P2, and 1.39 A/m in P3. The remainder of the model consists of rectangular prism, P4, taken from Whitehill, and 8-sided prism, P5, similar to the lowermost cylinder of Allingham and Zietz. Computations with a three-dimensional forward program, and comparisons with anomalies along the two traverses, assigned a magnetization of 1.55 A/m to prisms P4 and P5. Computed anomalies for the model closely resemble the observed residual anomalies along traverse A63-A63' as shown in figure 14C (A).

Model computations and depth estimates from slope distances indicate that most of the stock anomaly arises from rocks at depths greater than 810 m (2,657 ft), the depth to the top of P4. The contribution of each of the five prisms to the 408 nT maximum on traverse A63-A63' is 5 nT from P1, 17 nT from P2, 24 nT from P3, 205 nT from P4, and 157 nT from P5. Most of the anomaly, therefore, comes from unsampled deep sources that could include strongly magnetized sedimentary rocks, as well as strongly magnetized granitic rocks.

FAULT INTERPRETATIONS

Interpretations of magnetic anomalies measured closer to the ground surface indicate major displacements of magnetized rock near the faults along the eastern and southeastern borders of stock exposures. The aeromagnetic map of figure 4C shows the circular stock anomaly 120 m (394 ft) above the surface, the mapped locations of major faults, and the positions of nine ground traverses. The residual anomalies of the map were compiled from aeromagnetic surveys flown about 120 m (394 ft) above the surface (Bath, 1976, and USGS, 1979). Unfortunately, the low-level aeromagentic data are incomplete in important areas along the eastern and southeastern sides of the stock.

The ground data were measured at 3-m (10-ft) intervals 1.5 m (5 ft) above the surface with a proton magnetometer. The ground magnetic anomalies over the stock and bordering faults are shown in east-west traverse A80-A80'

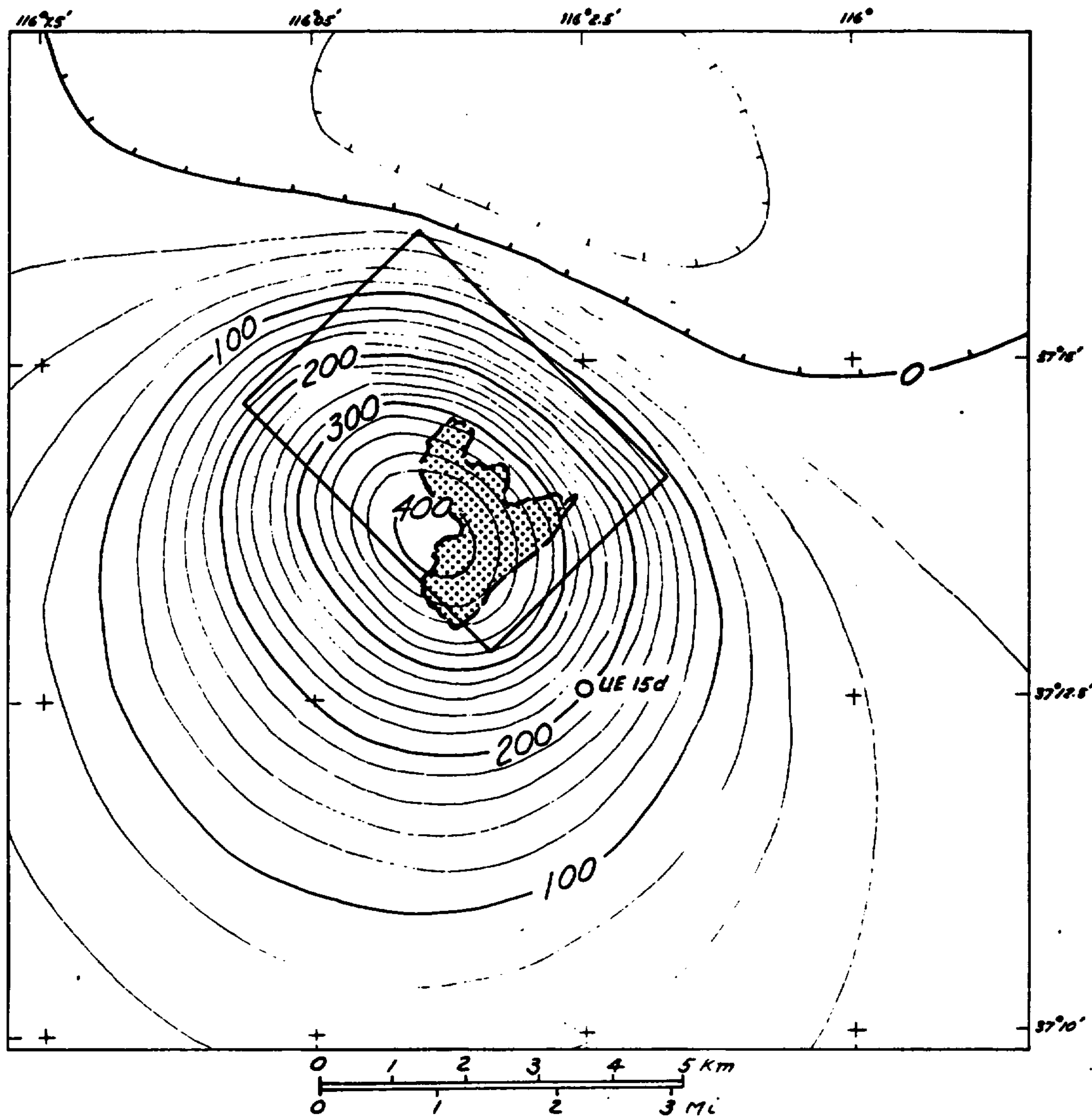

Figure 12C.--Rectangular outline of the vertical prism of Whitehill (1973) giving a computed anomaly that best fits the observed anomaly. Also shown and contoured at 20-nT interval is the anomaly computed for the prism which has a magnetization along the Earth's field at an intensity of 2.27 A/m. The prism is 4,840 m (15,900 ft) long, 3,430 m (11,250 ft) wide, and 17,200 m (56,400 ft) thick. The top of the prism has an elevation of 427 m (1,400 ft) which is 1,160 m (3,800 ft) below the elevation of the shaded outline of exposed granitic rocks. Drill hole UE15d is 1,250 m (4,100 ft) southeast of the prism.

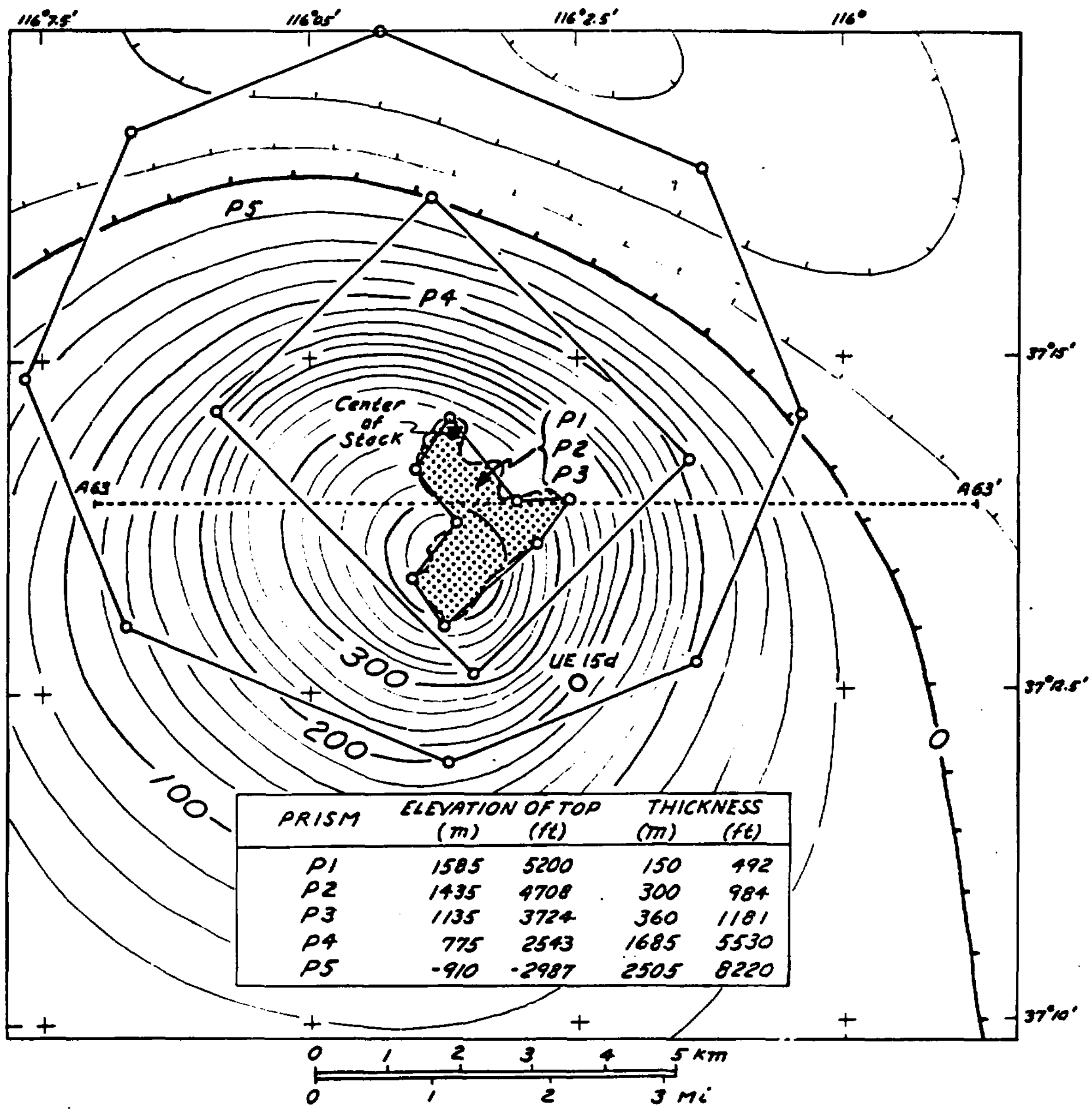

PRISM	ELEVATION OF TOP (m)	ELEVATION OF TOP (ft)	THICKNESS (m)	THICKNESS (ft)
P1	1585	5200	150	492
P2	1435	4708	300	984
P3	1135	3724	360	1181
P4	775	2543	1685	5530
P5	-910	-2987	2505	8220

Figure 13C.--Outlines and tabulated dimensions of the five vertical prisms used to explain the anomaly of figure 10C, and to represent the gross configuration of the stock. Also shown and contoured at 20-nT interval is anomaly computed for the prisms when magnetized along the Earth's field at an intensity that increases from 0.28 A/m for prism 1 to 1.55 A/m for prisms 4 and 5. Also shown are shaded outline of the exposed part of the stock, approximate center of the stock model, and air traverse A63-A63'.

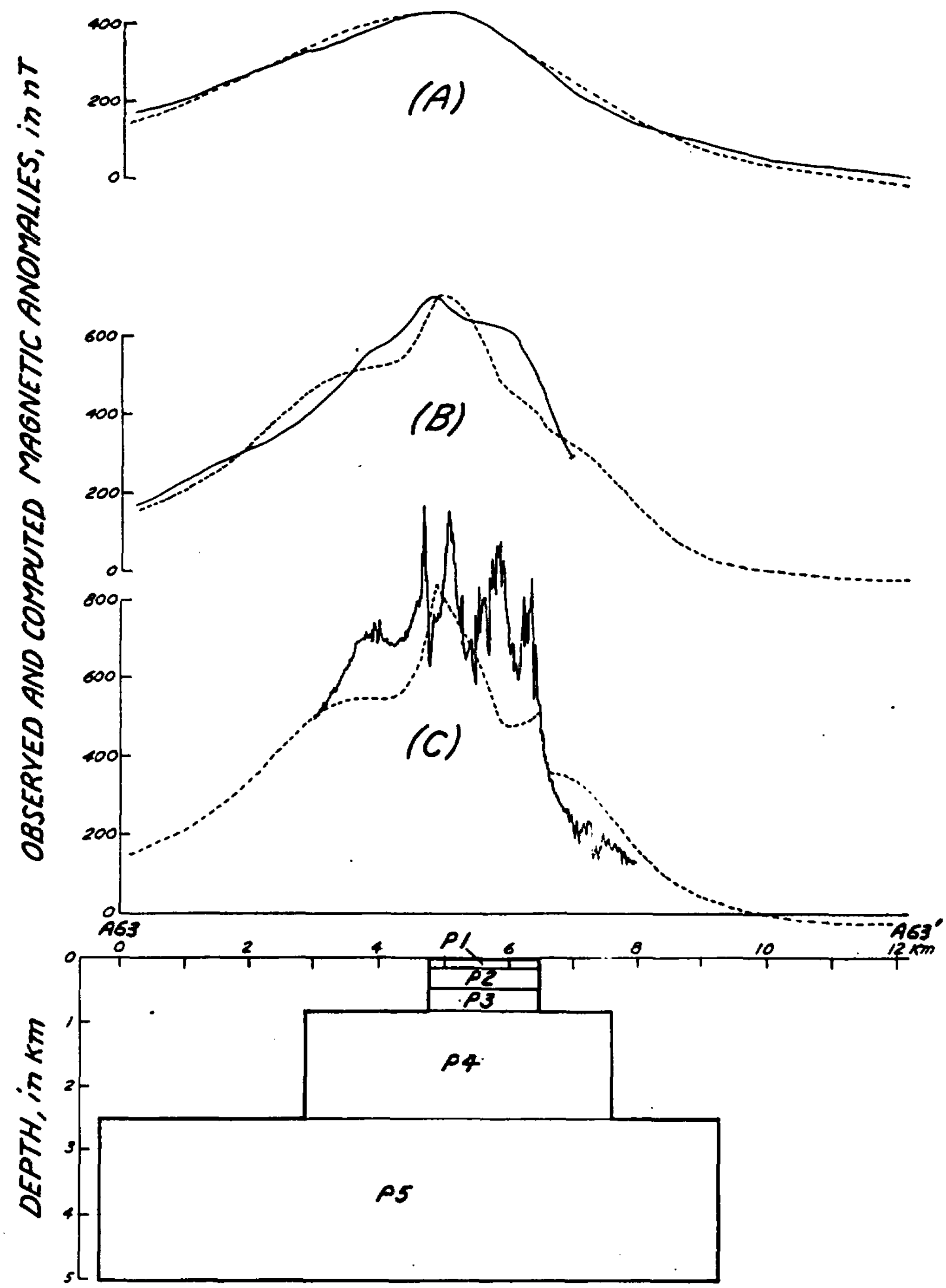

Figure 14C.--Section through the five prisms of figure 13C showing residual and computed anomalies along traverse A63-A63' at (A) 850 m (2,789 ft), (B) 120 m (394 ft), and (C) 1.5 m (5 ft) above the stock. Solid lines are residual anomalies, and dashed lines are computed anomalies.

positioned beneath air traverse A63-A63' (fig. 15C); B80-B80' parallel to and 305 m (1,000 ft) south of A80-A80' (fig. 15C); and C80-C80' to the northeast over the high topography to the north (fig. 16C). Five parallel traverses, A73-A73', B73-B73', C73-C73', D73-D73', and E73-E73', oriented N. 35° W. pass over the southeastern edge of the stock and the Boundary and Yucca faults (fig. 17C). In order to facilitate positional correlations, the ground anomalies are plotted above elevations of the topographic surface and a schematic representation of known faults and geologic units.

Slope distances and anomaly amplitudes provide a basis for estimates of magnetization, and thus for relating ground anomaly patterns to areal distributions of geologic units. Estimates are generally consistent with values from samples listed in tables 1, 2, and 3. Anomaly amplitudes are low, and application of equation (2) usually reveals nonmagnetic or weakly magnetic rocks. The only strongly magnetized rocks are in a granodiorite feature that is 200 m (656 ft) wide at the 85.0-km (52.8-mi) station on the truck-mounted magnetometer traverse shown on figure 9C. The prominent anomaly of more than 1,800 nT at the 2,900-m (9,514-ft) station of traverse C80-C80' (fig. 16C) is assumed to arise from concentrations of iron and steel objects in underground workings. Alluvium and most older sedimentary rocks are nonmagnetic, and most intrusive and all volcanic units are weakly magnetized. There are, however, local occurrences of moderately magnetized quartz monzonite, granodiorite, and sedimentary rocks.

Change of anomaly pattern, as well as distinctive anomalies are present near several faults and contacts, but many amplitudes are small because of weak magnetizations of near-surface rocks. There are minor changes over the Tippinip fault on traverses A80-A80' and B80-B80'; and over the Boundary and Butte faults on traverses A80-A80' and B80-B80'; and over the Boundary and Butte faults on traverse C80-C80'. A local positive anomaly of less than 100 nT is shown west of the Tippinip fault near station 4.0 km (2.5 mi) on traverse A63-A63' (C) of figure 14C, and near station 800 m on traverse A80-A80' of figure 15C. Also six traverses over the eastern and southeastern parts of the stock show the abrupt reductions in anomaly amplitude that are expected at stock edges or displaced magnetized rock. Anomaly decreases are present east of the Boundary fault (fig. 4C) on ground traverses A80-A80' and B80-B80' of figure 16C., and southeast of the Boundary fault (fig. 4C) on ground traverses B73-B73', C73-C73', D73-D73', and E73-E73' of figure 18C.

The computed contours and profiles of figures 13C and 14C illustrate the anomalies expected over the Climax stock, assuming it is bordered by fault-like vertical sides. Computations are for the gross configuration model of figure 13C, and the vertical sides extend to a depth of 810 m (2,658 ft), the combined thickness of prisms P1, P2, and P3. Data are computed at 850 m (2,789 ft), 120 m (394 ft), and 1.5 m (5 ft) above P1.

Boundary and Tippinip Faults

Structures near the Boundary and Tippinip faults were investigated by modifying the configuration and magnetization of the stock model (fig. 13C) in order to explain the local anomalies in ground magnetic traverses over edges of the stock. The stock model is constructed of vertical prisms that have polygonal outlines in plan view. The vertical prisms near the surface were replaced with horizontal prisms that have polygonal outlines in section view.

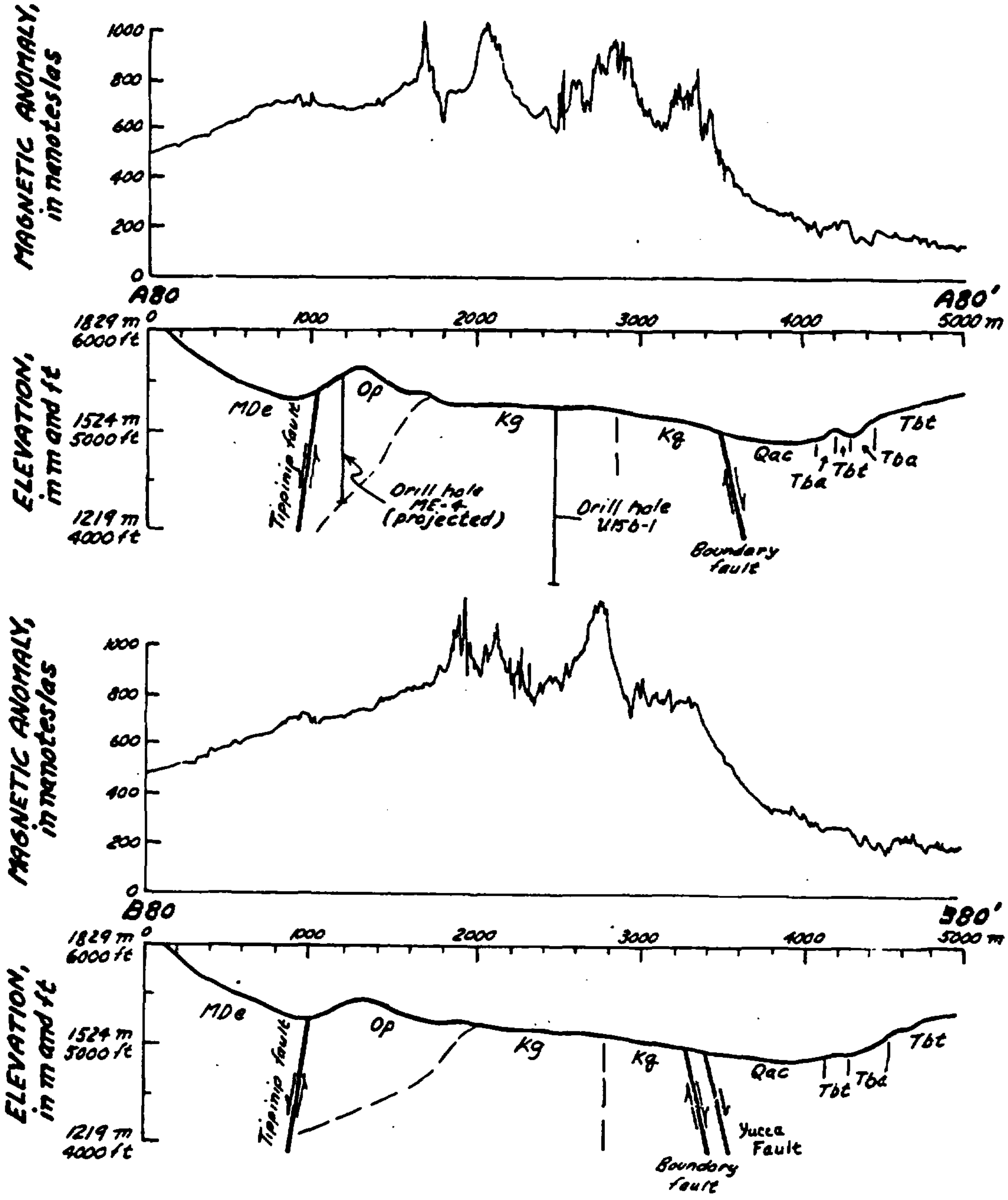

Figure 15C.--Profiles of residual ground magnetic anomalies along traverses A80-A80' and B80-B80' over Eleana Formation, MDe; Pogonip Group, Op; granodiorite stock, Kg; quartz monzonite stock, Kq; alluvium and colluvium, Qac; Tub Spring Member of the Belted Range Tuff, Tbt; air-fall, bedded, and zeolitized tuff, Tba; and Tippinip and Boundary faults. Each profile was plotted from 1,700 proton magnetometer measurements 1.8 m (6 ft) above ground surface.

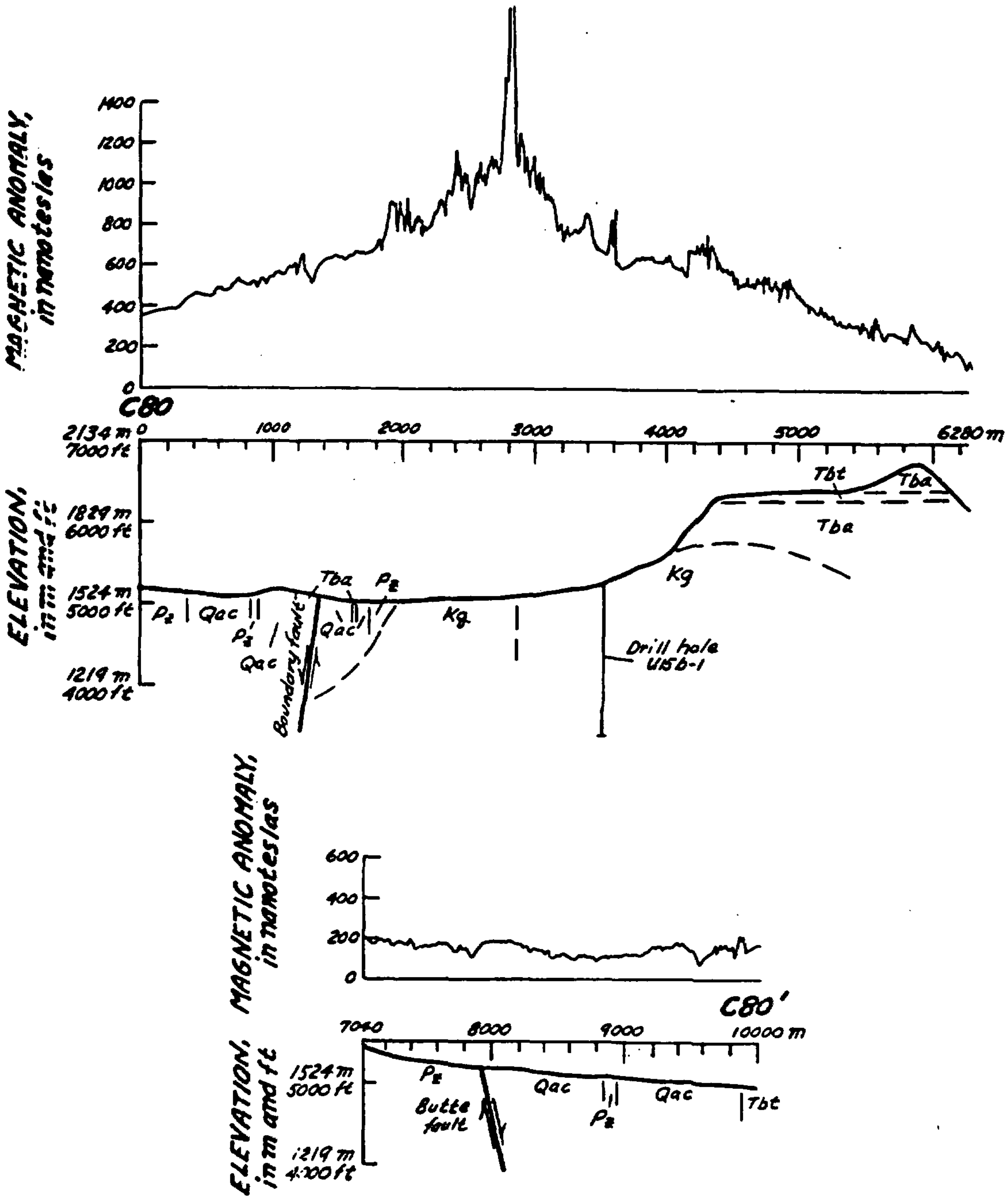

Figure 16C.--Profile of residual ground magnetic anomalies along traverse C80-C80' over Paleozoic sedimentary rocks, Pz; granodiorite stock, Kg; quartz monzonite stock, Kq; Tub Spring Member of the Belted Range Tuff, Tbt; air-fall, bedded, and zeolitized tuff, Tba; alluvium and colluvium, Qac; and Boundary and Butte faults. Profile was plotted from 3,000 proton magnetometer measurements 1.8 m (6 ft) above ground surface. No measurements were made over steep slope in interval 6,280 to 7,040 m (20,603-23,087 ft).

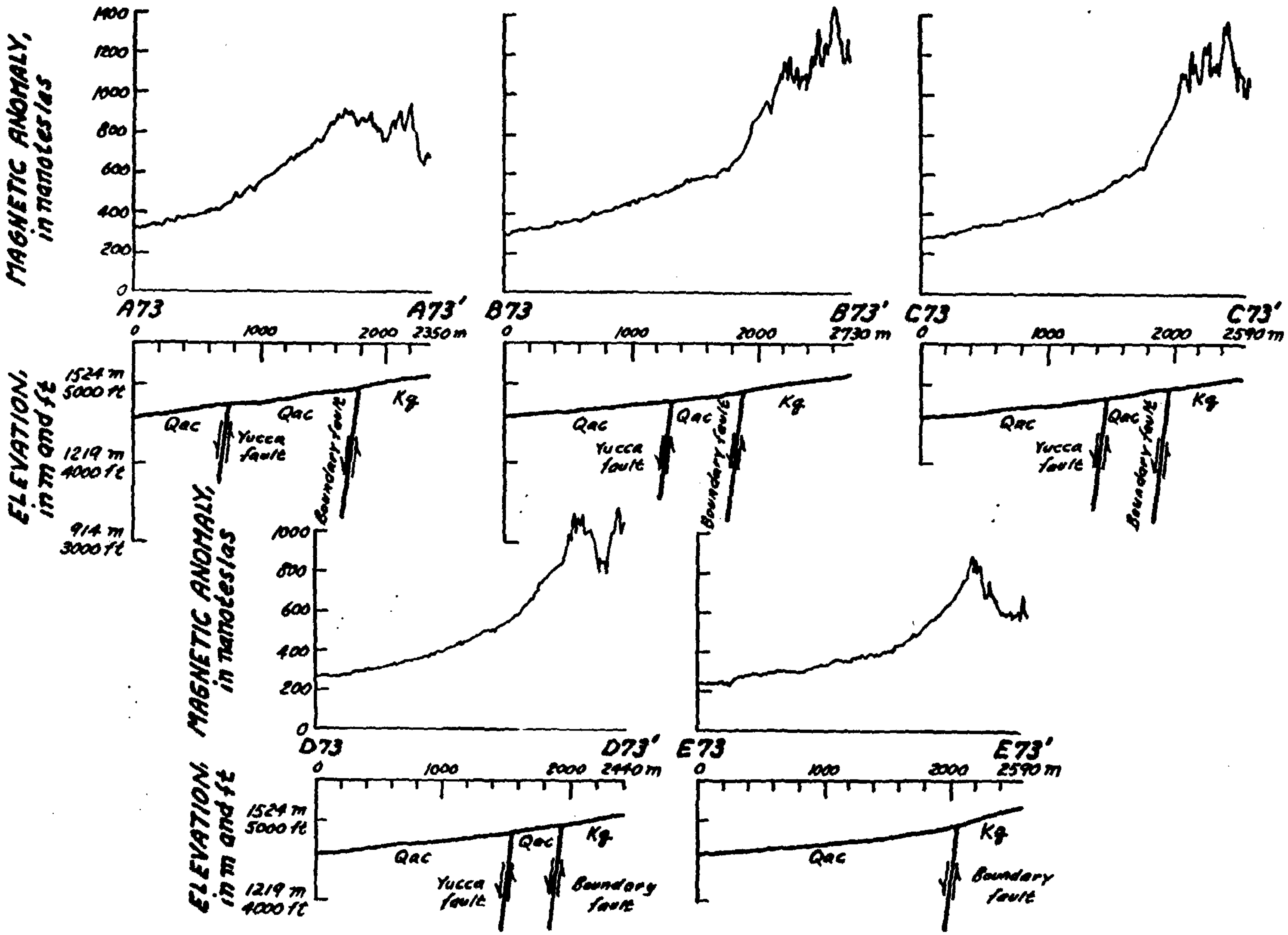

Figure 17C.--Profiles of residual ground magnetic anomalies along traverses A73-A73', B73-B73', C73-C73', D73-D73', and E73-E73' over quartz monzonite stock, Kq; alluvium and colluvium, Qac; and Yucca and Boundary faults. Profiles were plotted from 1,666 proton magnetometer measurements 1.4 m (4.6 ft) above ground surface.

This permitted use of several horizontal prisms of irregular outline to represent the relatively complex configurations of known and inferred geologic structure in section view. The cumulative effects of all vertical and horizontal prisms were then computed with a three-dimensional forward program and compared with the ground magnetic anomalies. Finally, several arrangements of prisms having different outlines and magnetizations were investigated to find the model judged most reasonable in terms of (1) comparisons of computed and measured anomalies, (2) surface and drill-hole geology, and (3) magnetic properties of core samples from nearby drill holes and magnetization estimates from ground magnetic anomalies.

The modified model of Climax stock at its southeastern edge is given on figure 18C along ground traverse C73-C73' (fig. 4C). The stock is represented by five prisms: horizontal prism P_H1 having J_t = 0.74 A/m, the average magnetization of quartz monzonite core from drill hole UE15f (table 3C); horizontal prisms P_H2, P_H3, and P_H4 having assigned magnetization of 1.55 A/m; and vertical prism P_V5 having assigned magnetization of 1.80 A/m. Southeast of the stock, alluvium is represented by horizontal prism Qac having a magnetization of 0 A/m indicated by estimates from the ground anomalies of figure 7C; volcanic rocks by horizontal prisms Tv having J_t = 0.30 A/m, the average of core from drill hole UE15d (table 1C); and metamorphosed sedimentary rocks of Precambrian age by horizontal prisms pCs having J_t = 0.10 A/m, a rough estimate from the limited core of drill hole UE15d (table 1C).

Almost all of the stock is terminated by the Boundary fault. This fault has high-angle southeastern dips of 80° to a depth of 750 m (2,461 ft) and 70° to a depth of 2,000 m (6,562 ft). A possible extension of the stock beyond the fault was investigated by replacing metamorphosed sedimentary rocks with granite in the wedge between the Boundary and Yucca faults. As shown on figure 18C, this resulted in poor comparison between residual and computed anomaly, and thus reduces the possibility of a significant extension to the southeast.

The modified model of Climax stock at its western edge is given in figure 19C along ground traverse A80-A80'. The stock is represented by five prisms: horizontal prism P_H1 having J_t = 0.85 A/m, the average magnetization of granite core from drill hole ME-4 (table 2C) plus the increase of 0.00196 A/m per meter of depth found in core from drill hole U15b-1 (fig. 6C); horizontal prism P_H2 having J_t = 1.30 A/m, resulting from continuing the increase of magnetization with depth; and horizontal prism P_H3, and vertical prisms P_V4 and P5, each having an assigned magnetization of 1.47 A/m. West of the stock, two groups of metamorphosed sedimentary rocks of Paleozoic age are present. The larger is represented by horizontal prism Pzs having J_t = 0.10 A/m, a rough estimate from variable core values of drill hole ME-4 (table 2C). The smaller group of unknown buried rocks is represented by the horizontal prism having an assigned J_t = 0.50 A/m and is defined by the dimensions given on figures 4C and 19C. The prism of unknown rock is required to explain the local magnetic high west of the fault.

The west edge of the stock dips 30° westward. The distinctive anomaly near the Tippinip fault is a local high, and not the reduction in anomaly amplitude expected west of a fault having its low-standing side to the west.

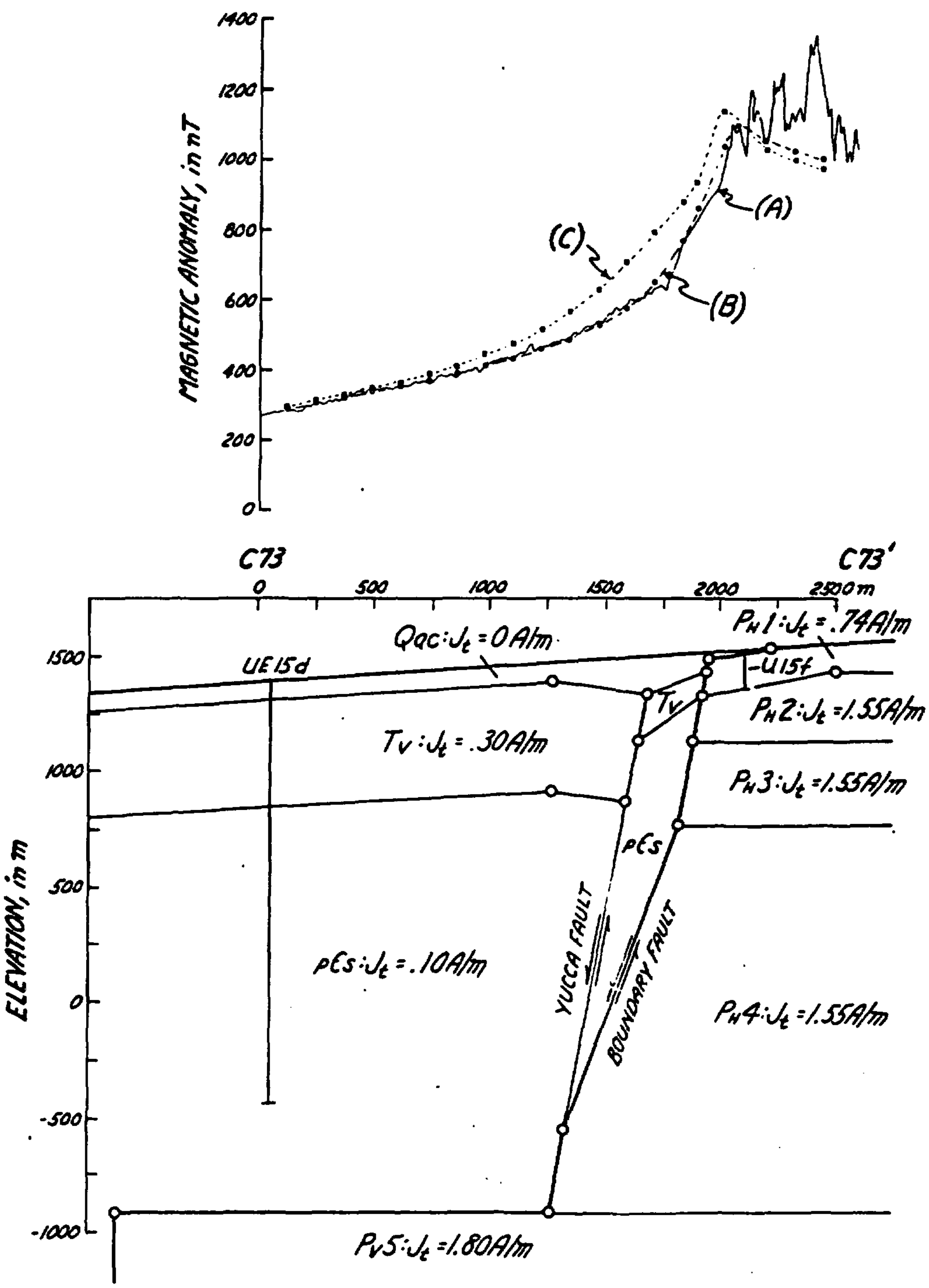

Figure 18C.--Section along ground traverse C73-C73' showing model selected to portray the southeastern edge of the stock. The stock is represented by prisms P_H1, P_H2, P_H3, P_H4, and P_V5; the Quaternary alluvium by prism Qac; the Tertiary volcanic rocks by prism Tv; and the Precambrian metasedimentary rocks by prism pCs. Also shown are Boundary and Yucca faults, and the rocks penetrated by drill holes UE15d and UE15f. Anomalies shown along the traverse are (A) measured residuals, (B) computed effects of the model, and (C) computed effects of the model with the modification of replacing metasedimentary rocks having J_t = 0.10 A/m with granitic rocks having J_t = 1.55 A/m in the wedge between Yucca and Boundary faults.

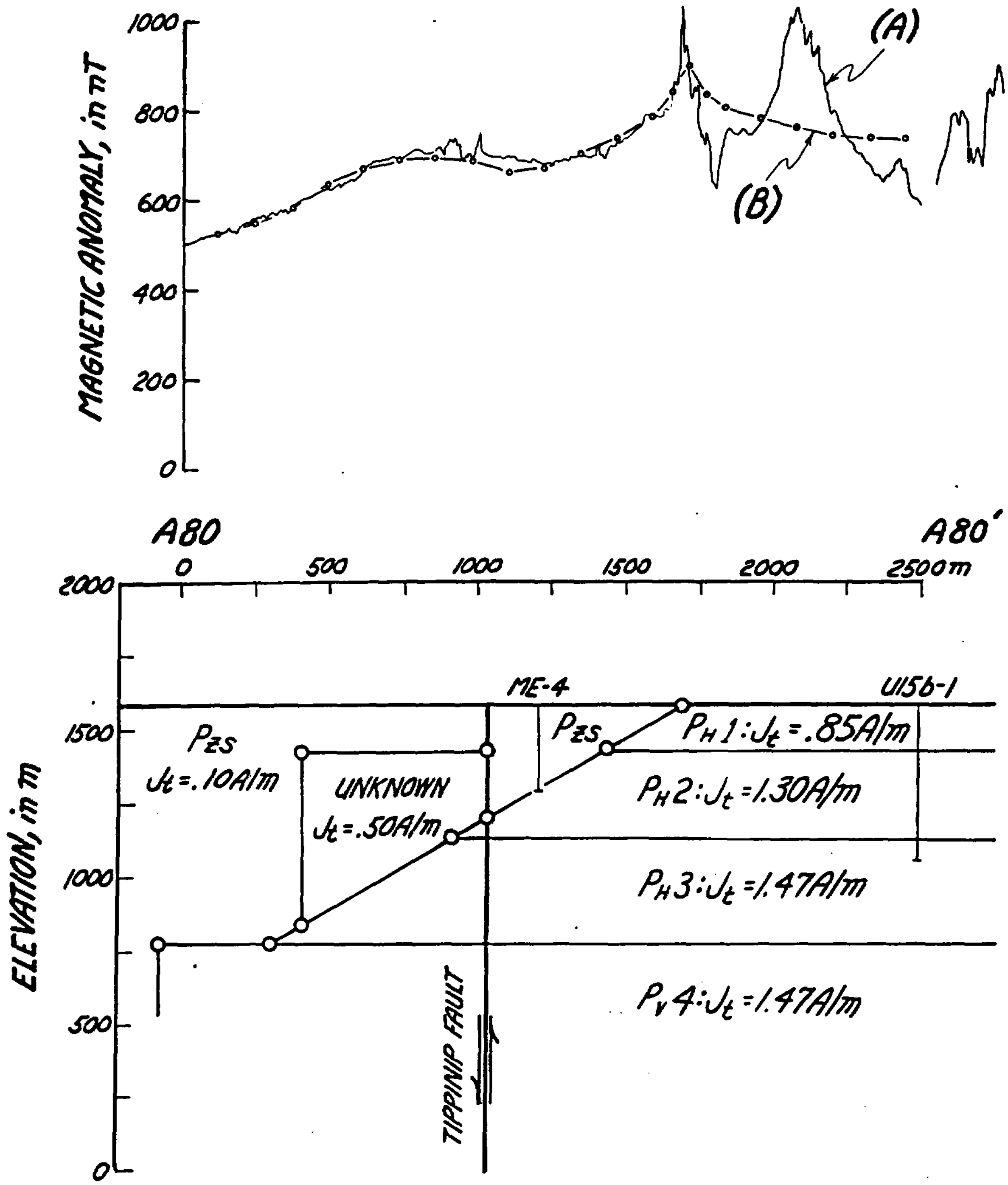

Figure 19C.--Section along ground traverse A80-A80' showing model selected to portray the western edge of the stock. The stock is represented by prisms P_H1, P_H2, P_H3, P_V4, and P5 (fig. 13C); the metasedimentary rocks by prism Pzs; and the unknown buried rocks by the prism having J_t = 0.50 A/m. Also shown is the Tippinip fault, and the rocks penetrated by drill holes ME-4 and U15b-1. Anomalies shown along the traverse are (A) measured residuals, and (B) computed effects of the model.

The unknown buried rocks may be Eleana Formation with an increased magnetite content similar to that observed near Calico Hills (Baldwin and Jahren, 1982), rather than magnetized granitic rock, and we are, therefore, unable to provide an interpretation of displaced granitic rock at the fault. The evidence for identifying the buried rock comes from amplified residual anomalies shown along traverses A80-A80' and B80-B80' on figure 20C. Slope distances indicate that near-surface Eleana Formation is magnetized just west of the Tippinip fault. Thus the Tippinip fault does not appear to bound the west edge or the stock in a fashion similar to the Boundary fault.

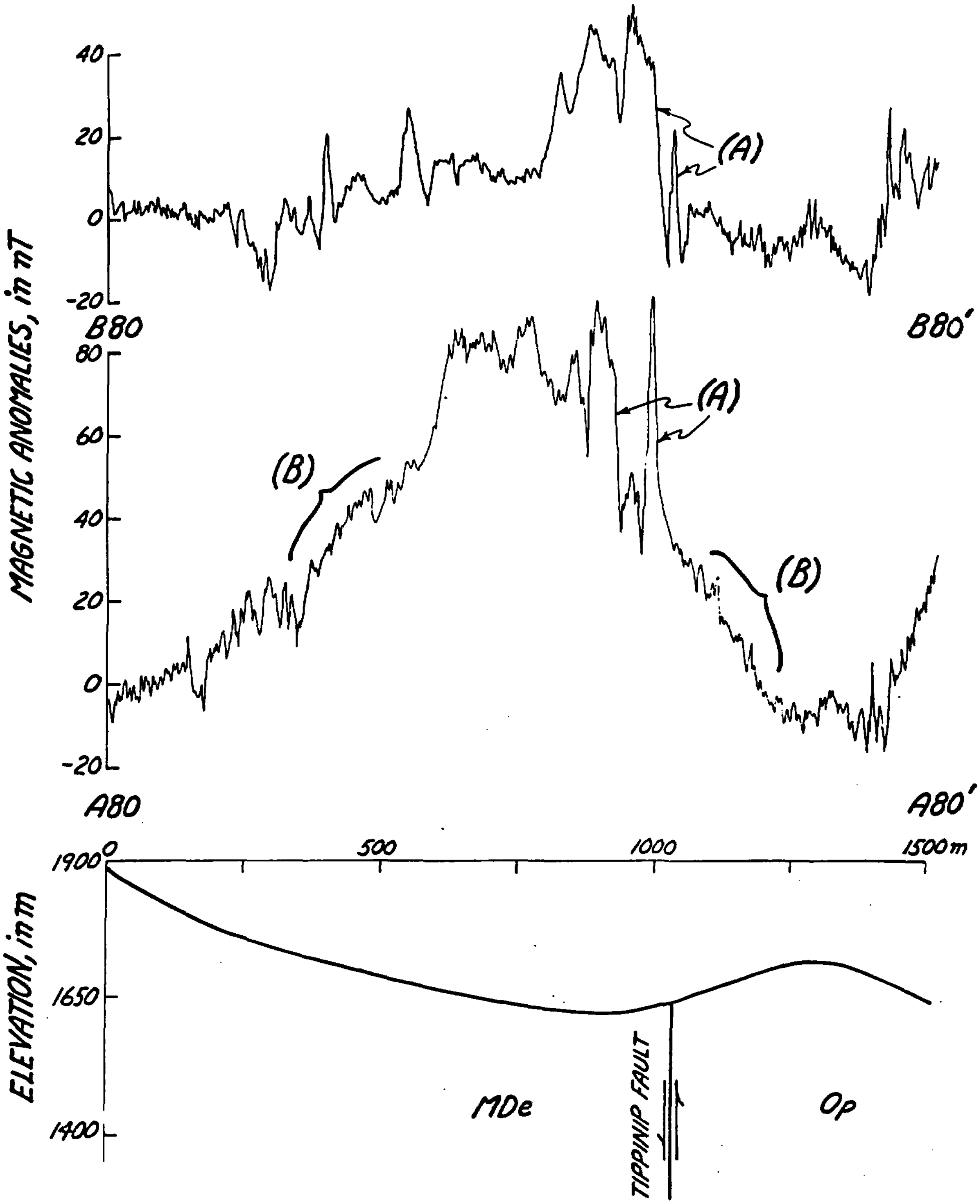

Figure 20C.--The amplified residual anomalies along traverses A80-A80' and B80-B80' showing slope distances that designate sources within 20 m (65 ft) (A) and 150 m (490 ft) (B) of the surface. Also shown are Tippinip fault, metamorphosed sedimentary rocks of the Eleana Formation, MDe, and metamorphosed sedimentary rocks of the Pogonip Group, Op. The shallow sources are just west of the Tippinip fault in the Eleana Formation, MDe.

REFERENCES CITED

Allingham, J. W., and Zietz, Isidore, 1962, Geophysical data on the Climax stock, Nevada Test Site, Nye County, Nevada: Geophysics, v. 27, p. 599-610.

Baldwin, M. J., and Jahren, C. E., 1982, Magnetic properties of drill core and surface samples from the Calico Hills area, Nye County, Nevada: U.S. Geological Survey Open-File Report 82-536, 27 p.

Barnes, Harley, Christiansen, R. L., and Byers, F. M., Jr., 1965, Geologic map of the Jangle Ridge quadrangle, Nye and Lincoln Counties, Nevada: U.S. Geological Survey Geologic Quadrangle Map GQ-363, scale 1:24,000.

Barnes, Harley, Houser, F. N., and Poole, F. G., 1963, Geology of the Oak Spring quadrangle, Nye County, Nevada: U.S. Geological Survey Geologic Quadrangle Map GQ-214, scale 1:24,000.

Barraclough, D. R., and Fabiano, E. B., 1978, Grid values and charts for the International Geomagnetic Reference Field 1975: U.S. Geological Survey Report PB-276 630, 139 p.; available only from U.S. Department of Commerce, National Technical Information Service, Springfield, VA 22161.

Bath, G. D., 1968, Aeromagnetic anomalies related to remanent magnetism in volcanic rock, Nevada Test Site, Nevada, in Nevada Test Site: Geological Society of America Memoir 110, p. 135-146.

_____1976, Interpretation of magnetic surveys in intermontane valleys at Nevada and southern New Mexico: U.S. Geological Survey Open-File Report 76-440, 36 p.

Boynton, G. R., Meuschke, J. L., and Vargo, J. L., 1963a, Aeromagnetic map of the Timber Mountain Quadrangle and part of the Silent Canyon Quadrangle, Nye County, Nevada: U.S. Geological Survey Geophysical Investigations Map GP-443, scale 1:62,500.

_____1963b, Aeromagnetic map of the Tippipah Spring Quadrangle and parts of the Papoose Lake and Wheelbarrow Peak Quadrangles, Nye County, Nevada: U.S. Geological Survey Geophysical Investigations Map GP-441, scale 1:62,500.

Boynton, G. R., and Vargo, J. L., 1963a, Aeromagnetic map of the Cane Spring Quadrangle and parts of Frenchman Lake, Specter Range, and Mercury Quadrangles, Nye County, Nevada: U.S. Geological Survey Geophysical Investigations Map GP-442, scale 1:62,500.

_____1963b, Aeromagnetic map of the Topopah Spring Quadrangle and part of the Bare Mountain Quadrangle, Nye County, Nevada: U.S. Geological Survey Geophysical Investigations Map GP-440, scale 1:62,500.

Byers, F. M., Jr., Carr, W. J., Orkild, P. P., Quinlivan, W. D., and Sargent, K. A., 1976, Volcanic suites and related cauldrons of Timber Mountain-Oasis Valley caldera complex, southern Nevada: U.S. Geological Survey Professional Paper 919, 70 p.

Carr, W. J., and Quinlivan, W. D., 1966, Geologic map of the Timber Mountain quadrangle, Nye County, Nevada: U.S. Geological Survey Quadrangle Map GQ-503, scale 1:24,000.

Christie, K. W., and Symons, D. T. A., 1969, Apparatus for measuring magnetic susceptibility and its anisotropy: Geological Survey of Canada, Paper 69-41, 10 p.

Currie, R. G., Gromme, C. S., and Verhoogan, Jean, 1963, Remanent magnetization of some Upper Cretaceous granitic plutons in the Sierra Nevada, California: Journal of Geophysical Research, v. 68, p. 2263-2279.

Ekren, E. B., and Sargent, K. A., 1965, Geologic map of the Skull Mountain quadrangle, Nye County, Nevada: U.S. Geological Survey Geologic Quadrangle Map GQ-387, scale 1:24,000.

Ekren, E. B., Orkild, P. P., Sargent, K. A., and Dixon, G. L., 1977, Geologic map of Tertiary rocks, Lincoln County, Nevada: U.S. Geological Survey Miscellaneous Geologic Investigations Map I-1041, scale 1:250,000.

Gibbons, A. B., Hinrichs, E. N., Hansen, W. R., and Lemke, R. W., 1963, Geology of the Rainier Mesa quadrangle, Nye County, Nevada: U.S. Geological Survey Geologic Quadrangle Map GQ-215, scale 1:24,000.

Gromme, C. S., and Merrill, R. T., 1965, Paleomagnetism of Late Cretaceous granitic plutons in the Sierra Nevada, California: Further results: Journal of Geophysical Research, v. 70, p. 3407-3420.

Henderson, R. G., and Zietz, Isidore, 1949, The upward continuation of anomalies in total magnetic intensity fields: Geophysics, v. 14, no. 4, p. 517-534.

Henderson, R. G., 1960, Polar charts for evaluating magnetic anomalies of three-dimensional bodies, in U.S. Geological Survey Short Papers in Geological Sciences: U.S. Geological Survey Professioanl Paper 400-B, p. B112-B114.

Houser, F. N., and Poole, F. G., 1960, Preliminary geologic map of the Climax stock and vicinity, Nye County, Nevada: U.S. Geological Survey Miscellaneous Investigations Map I-328, scale 1:4,800.

Jahren, C. E., and Bath, G. D., 1967, Rapid estimation of induced and remanent magnetization of rock samples, Nevada Test Site: U.S. Geological Survey Open-File Report, 29 p.

Kane, M. F., Harwood, D. S., and Hatch, N. L., Jr., 1971, Continuous magnetic profiles near ground level as a means of discriminating and correlating rock units: Geological Society of America Bulletin, v. 82, p. 2449-2456.

Koenigsberger, J. G., 1938, Natural residual magnetism of eruptive rocks: Terrestrial Magnetism and Atmospheric Electricity, v. 43, p. 119-299.

McKay, E. J., and Williams, W. P., 1964, Geology of the Jackass Flats quadrangle, Nye County, Nevada: U.S. Geological Survey Quadrangle Map GQ-368, scale 1:24,000.

Nettleton, L. L., 1976, Gravity and magnetics in oil prospecting, in International series in the Earth and planetary sciences: McGraw-Hill, New York, 464 p.

Noble, D. C., and Christiansen, R. L., 1968, Geologic map of the southwest quarter of the Black Mountain quadrangle, Nye County, Nevada: U.S. Geological Survey Miscellaneous Geologic Investigations Map I-562, scale 1:24,000.

Oliver, H. W., 1977, Gravity and magnetic investigations of the Sierra Nevada batholith, California: Geological Society of America Bulletin, v. 88, p. 445-461.

Philbin, P. W., and White, B. L., Jr., 1965a, Aeromagnetic map of parts of the Cactus Peak and Stinking Spring quadrangles, Nye County, Nevada: U.S. Geological Survey Geophysical Investigations Map GP-517, scale 1:62,500.

_____ 1965b, Aeromagnetic map of parts of the Kawich Peak and Reveille Peak quadrangles, Nye County, Nevada: U.S. Geological Survey Geophysical Investigations Map GP-516, scale 1:62,500.

Philbin, P. W., and White, B. L., Jr., 1965c, Aeromagnetic map of the Cactus Spring quadrangle and part of the Goldfield quadrangle, Esmeralda and Nye Counties, Nevada: U.S. Geological Survey Geophysical Investigations Map GP-511, scale 1:62,500.

_____1965d, Aeromagnetic map of the Mellan quadrangle, Nye County, Nevada: U.S. Geological Survey Geophysical Investigations Map GP-518, scale 1:62,500.
_____1965e, Aeromagnetic map of the Quartzite Mountain quadrangle, Nye County, Nevada: U.S. Geological Survey Geophysical Investigations Map GP-515, scale 1:62,500.
_____1965f, Aeromagnetic map of the Belted Peak quadrangle and part of White Blotch Springs quadrangle, Nye County, Nevada: U.S. Geological Survey Geophysical Investigations Map GP-514, scale 1:62,500.
_____1965g, Aeromagnetic map of the Sarcobatus Flat area, Esmeralda and Nye Counties, Nevada: U.S. Geological Survey Geophysical Investigations Map GP-512, scale 1:125,000.
_____1965h, Aeromagnetic map of the Black Mountain quadrangle, Nye County, Nevada: U.S. Geological Survey Geophysical Investigations Map GP-519, scale 1:62,500.
_____1965i, Aeromagnetic map of the Silent Canyon quadrangle, Nye County, Nevada: U.S. Geological Survey Geophysical Investigations Map GP-520, scale 1:62,500.
_____1965j, Aeromagnetic map of the Wheelbarrow Peak quadrangle and part of the Groom Mine quadrangle, Nye and Lincoln Counties, Nevada: U.S. Geological Survey Geophysical Investigations Map GP-513, scale 1:62,500.
Rodgers, C. L., Anderson, R., E., Ekren, E. B., and O'Connor, J. T., 1967, Geologic map of the Quartzite Mountain quadrangle, Nye County, Nevada: U.S. Geological Survey Geologic Quadrangle Map GQ-672, scale 1:24,000.
Rosenbaum, J. G., Larson, E. E., Hoblitt, R. P., and Fickett, F. R., 1979, A convenient standard for low field susceptibility calibration: Review of Scientific Instruments, v. 50, p. 1027-1029.
Sargent, K. A., and Orkild, P. P., 1973, Geologic map of the Wheelbarrow Peak-Rainier Mesa area, Nye County, Nevada: U.S. Geological Survey Miscellaneous Geologic Investigations Map I-754, scale 1:48,000.
Smith, R. A., 1961, Some theorems concerning local magnetic anomalies: Geophysical Prospecting, v. 9, p. 399-410.
Sweeney, R. E., Godson, R. H., Hassemer, J. H., Dansereau, D. A., and Bhattacharyya, B. K., 1978, Composite aeromagnetic map of Nevada: U.S. Geological Survey Open-File Report 78-695, scale 1:500,000.
U.S. Geological Survey, 1979, Aeromagnetic map of the Timber Mountain area, Nevada: U.S. Geological Survey Open-File Report 79-587, scale 1:62,500.
Vacquier, Victor, Steenland, N. C., Henderson, R. G., and Zietz, Isidore, 1951, Interpretation of aeromagnetic maps: Geological Society of America Memoir 47, 151 p.
Whitehill, D. E., 1973, Automated interpretation of magnetic anomalies using the vertical prism model: Geophysics, v. 38, p. 1070-1087.
Zietz, Isidore, Stewart, J. H., Gilbert, F. P., and Kirby, J. R., 1977, Aeromagnetic map of Nevada: U.S. Geological Survey Miscellaneous Field Investigations Map MF-902, scale 1:500,000.